CENTRO DE INVESTIGACIONES EN ÓPTICA, A.C.

Design, Fabrication and Characterization of Nonlinear Photonic Crystal Fibers for Near Infrared Wavelength Supercontinuum Light Sources

(Final version. Include changes suggested by reviewers)

Maestría en Optomecatrónica

(Master of Optomechatronics)

Adviser: Dr. Uladzimir Petrovich Minkovich

Student: Eng. Carlos Enrique Porras Barajas

October, 2017

León, Guanajuato, México

Design, Fabrication and Characterization of Nonlinear Photonic Crystal Fibers for Near Infrared Wavelength Supercontinuum Light Sources

By

Carlos Enrique Porras Barajas

Approved by:

Dr. Alexander Kir'yanov
Examiner

Dr. Roberto Ramírez Alarcón
Examiner

Dr. Uladzimir Petrovich Minkovich
Examiner

Contents

Acknowledments

I would like to thank my parents, Margarita and Enrique, for their support in all my academic development and for their unconditional love, as well as my sister, Estefanía; without them this would not have been possible.

To Laura, for all the joy and support you have given me in all these years. You gave me the strength to continue till the end, thank you my beloved fiancée.

To my advisor, Dr. Uladzimir P. Minkovich, for all his patience and guidance along my thesis work.

To Dr. Alexander Kir'yanov and Dr. Roberto Ramírez for taking the time to read this work and for their useful feedback.

To Centro de Investigaciones en Óptica, for giving me the opportunity to study in its facilities and for providing the necessary resources to develop my skils.

Finally, to CONACYT, for its financial support which allowed me to finish my studies.

Resume

Optical fiber is one of the most exploited invention in the last century, both in research and technology. In the last years a new kind of optical fiber has been fabricated and investigated with a name of Photonic Crystal Fiber (PCF). The PCFs are fibers with a periodic arrangement of low index material in a background with higher refractive index. Usually, pure silica is the background material and the low index region is given by air holes.

Among all kind of PCFs, there is a type of PCFs, in which high nonlinear effects are easily induced. These fibers are called Highly Nonlinear Photonic Crystal Fibers (HNL PCFs), and they are fabricated and studied in this work.

The fabrication of a HNL PCF is more complicated process than fabrication of conventional optical fibers. At the first time a design of a preform is calculated. There are several preform fabrication techniques, such as drilling, extrusion, casting and stacking; each of them is suitable for a specific preform material. In CIO, the stack and draw technique is used to fabricate the preforms. At the first time needed capillaries, special packers of different diameters and a solid core rod are drown. The fabricated capillaries and packers are arranged carefully in a hexagonal structure around the core rod giving a stack. The stack is then drawn into canes with needed outside diameters. To draw a fiber, a cane is inserted into a jacketing tube. This construction is drawn then into a HNL PCF.

In this thesis, all the stages at fabrication of HNL PCFs are carried out, starting from PCF design at using of special relations and finishing to HNL PCF fabrication.

Once the fiber is made, it is necessary to characterize it. Some of the most important parameters are dispersion, attenuation, beam divergence and numerical aperture. We present the appropriate way to compute the parameters and then to fabricate of the calculated HNL PCFs. Finally, we expose the

relevance of the design and fabrication of HNL PCF for specific applications, such as supercontinuum generation.

Goal

To develop an improved fabrication of high nonlinear index guiding silica photonic crystal fibers (HNL IG PCFs) for near infrared wavelength supercontinuum light sources and to make detailed investigations of HNL IG PCF optical properties.

Objectives

The objectives of the present work are listed below:

1. *To become familiar with theoretical and experimental methods of HNL IG PCF studying.*
2. *To develop an improved fabrication of composite silica preforms for drawing of HNL IG PCFs.*
3. *To improve regimes for drawing of developed HNL IG PCFs.*
4. *To make detailed investigations of fabricated HNL IG PCF properties.*
5. *To present MS degree thesis before the end of the project.*

Introduction

The unique property of index-guiding photonic crustal fibers (IG PCFs) lies in the possibility to control chromatic dispersion in such fibers within a wide wavelength range by varying a hole diameter d and a hole-to-hole spacing, pitch Λ. To date, high nonlinearity IG PCFs (HNL IG PCFs) with zero dispersion wavelength in the visible and near-infrared wavelengths [1-4], with two zero dispersions [5-6], with varying dispersion [7-8], with flattened and near zero dispersion [9-11] have been reported. The well-known publications describing supercontinuum generation (SC) in IG PCFs mainly dealt with PCFs with a large number of hole rings in a regular cladding, which is a two-dimensional photonic crystal, and usually only the fundamental mode of the fiber was involved in SC [2, 12].

Single-mode guidance in IG PCFs with suitable dispersive properties, however requires fibers with a (sub)wavelength-sized core diameter, in which the material damage threshold typically limits the maximum achievable power spectral density to a few mW/nm for ultrashort pulse operation [13] and for more than 50 mW/nm for CW operation [14]. In the ultrashort pulse regime, where the fiber damage rather than the available pump laser power represents the limiting factor, possible employing fibers with a larger core, operating in a multimode regime, represents the obvious solution to increase the achievable power spectral density. Moreover, apart from high-power handling, multimode fibers also possibly may exhibit a variety of novel nonlinear phenomena.

In the current work, we present fabrication of special high nonlinear, index guiding silica photonic crystal fibers (single-mode and multimode) for near infrared wavelength supercontinuum light sources. We fabricated PCFs with different core diameters, different zero dispersion wavelengths, different numbers of air hole rings in a PCF cladding and with long length. Detailed investigations of fabricated HNL IG PCF optical properties were carried out. For comparing,

we also investigated a special HNL IG PCFs with a core doped with germanium (Ge), manufactured in Central Glass & Ceramic Research Institute, Calcutta, India.

Chapter 1
Introduction to Photonic Crystal Fibers

When we hear the term "optical fiber", the first thought in our mind is a solid thread surrounded by another material with a lower refractive index. However, photonic crystal fibers (PCFs) are established as an alternative fiber technology. PCFs are optical fibers with a periodic arrangement of low index material in a background with higher refractive index. The most common high refractive index background material is pure silica and the low index region is provided by air holes running along the entire length [15].

Before explaining the properties of PCFs, a review of conventional optical fibers is presented.

1.1 Conventional Optical Fibers

An optical fiber is a cylindrical waveguide that can transmit light from one point to another, in the same way a copper wire guides electrical signals. It consists of

a cylindrical central dielectric core, surrounded by a dielectric material of a slightly lower refractive index [16]. The conventional optical fiber, used widely in modern telecommunications, has another protective layer, called coating or jacket.

Silica is the most common material used for the fabrication of optical fibers. Some dopants are used to increase the refractive index of the core, such as germanium. With this refractive index difference, light coupled into the core can travel along the fiber, as is explained in the next section.

1.1.1Guidance mechanism

Traditional optical fiber relies on total internal reflection to guide light. Since the core has a refractive index larger than the cladding, total internal reflection can be achieved at the edge of both interfaces. However, only certain incident angles are allowed.

1.1.2Acceptance angle and numerical aperture

The acceptance angle and numerical aperture are critical characteristics of optical fibers used to describe the angles associated with light propagation. The acceptance angle is the angular cone of light, which is transmitted along the fiber. The sine of the half-angle of this angle is known as the numerical aperture (NA) [17]. These parameters can be related to the refractive indices of the fiber materials by using Snell's law. Figure 1.1 illustrates the parameters explained above.

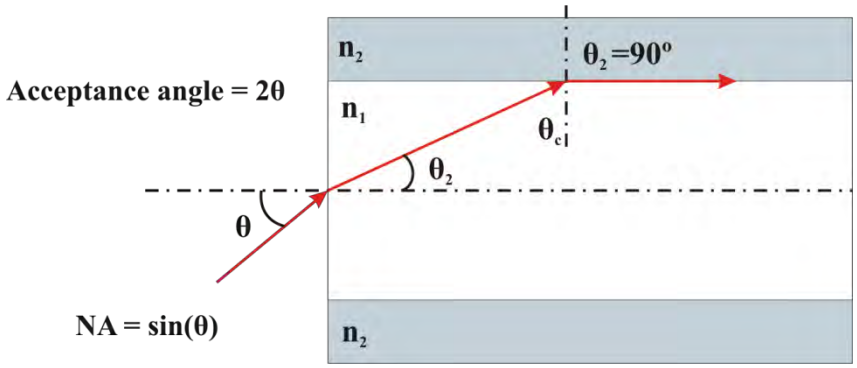

Figure 1.1 Numerical aperture and acceptance angle in an optical fiber.

Using the parameters of Figure 1.1, the NA can be computed using the Equation 1.1.

$$NA = \sin(\theta) = \sqrt{n_1^2 - n_2^2} \tag{1.1}$$

Where n_1 and n_2 are the refractive indices of the core and the cladding respectively.

1.1.3Fiber modes

The numerical aperture implies that any acceptance angle between normal incidence and the acceptance half-angle will propagate within the fiber, but the geometry of the fiber and the existence of forward-traveling and backward-traveling waves yield constructive and destructive wave interference, allowing only certain ray angles or modes to propagate [17].

As we can imagine, mode theory uses electromagnetic wave behavior to describe how the light propagates through an optical fiber. A set of guided electromagnetic wave is called the modes of the fiber. To know how many modes a fiber can support, a new concept is introduced: the normalized frequency V or V-number. Its mathematical expression is showed in Equation (1.2).

$$V = \frac{2\pi a}{\lambda}\sqrt{n_1^2 - n_2^2} \tag{1.2}$$

Where a is the core radius and λ is the wavelength of light in the air. The smaller this parameter, the smaller the number of guided modes the fiber can carry. If for a given wavelength $V < 2.405$, only one mode propagates: the fundamental mode. In that case, the fiber is said to be single-mode.

1.1.4Losses

The basic way to measure losses (or attenuation) in a system is to compare the energy before and after the process. Any system does not have one hundred

percent of efficiency, and optical fibers are not an exception. There are two main causes of losses in optical fiber: absorption and bending.

1.1.4.1 Absorption losses

In an ideal fiber, the attenuation of a guided mode is due to material absorption. If the material was completely lossless, then the guided mode would not be attenuated at all. The absorption of pure silica is very small in a wavelength range of 800 nm and 1800nm [18], so it is possible to have almost the same power signal along all the fiber. In case impurities are present within the fiber, absorption losses will increase.

However, absorption by the hydroxyl group OH is not negligible, where its main absorption peak is centered at 1380 nm [19].

1.1.4.2 Bending losses

If an optical fiber is bent, the guided light in the core may become unguided, producing loss of power. This phenomenon is produced when a fiber is bent into a circular arc, then the light propagating within the core will strike the core-cladding at the bending point, making an angle θ with the surface normal at that point. If the arc is strong, θ will become smaller than the critical angle, and the light will no longer be guided [20].

Those losses can disappear when the bending is removed, but if the bending is produced in a micro scale, *i. e.* fabrication or stress damage, the losses are permanent.

1.1.5Dispersion

In optical fibers, dispersion is the spreading out of a light pulse in time as it propagates down the fiber [21]. This phenomenon is highly undesirable in telecommunications systems because it reduces the useful bandwidth of the fiber.

In more detail, the dispersion is sorted into four main categories: multimode or modal, material, waveguide and polarization mode dispersion [22].

1.1.5.1 Multimode or modal dispersion

Each propagating mode in an optical fiber has a different group velocity. In a multimode fiber, this effect produces waveform distortion, and the effect is amplified with the length of the fiber.

The intuitive solution to avoid modal dispersion is using single-mode fibers, where this effect is absent.

1.1.5.2 Material dispersion

In any material, the refractive index has a dependency of the light frequency. Spectrally, a light pulse has a finite frequency bandwidth; i. e. the light pulse is the superposition of a range of frequencies. Then, each frequency will travel at a different velocity, generating a waveform distortion. The delay distortion produced in this case is called material dispersion.

1.1.5.3 Waveguide dispersion

Even when we consider that material dispersion is absent, the delay distortion due to the finite frequency bandwidth would remain because the mode group velocity is generally a function of frequency [23]. The waveform distortion caused by this effect is called waveguide dispersion.

1.1.5.4 Polarization mode dispersion

Polarization dispersion is due to fiber imperfections, which cause disturbances in the symmetry of the fiber core [24]. If the fiber core does not have a perfect circular aperture, polarization mode dispersion arises from the preferential polarization modes along a perpendicular axis, as shown in Figure 1.2.

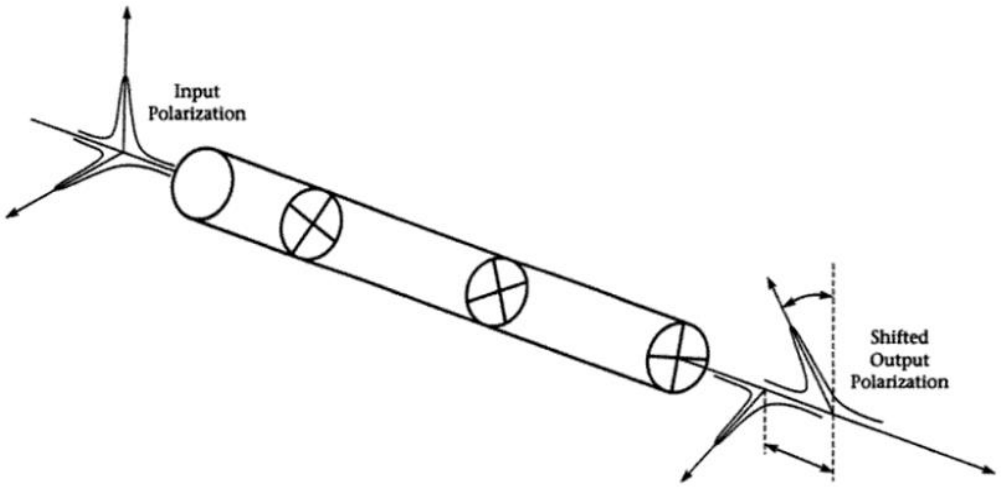

Figure 1.2 Polarization mode dispersion. Courtesy of [24].

1.2 Photonic Crystal Fibers

So far we have been talking about conventional optical fibers and their main properties, but recently a new type of fiber has been studied: photonic crystal fibers.

The photonic bandgap effect was first described in 1987 by Yablonovitch and John [25, 26], who studied spontaneous emission control and localization of light in novel periodic materials. The name photonic crystals (or photonic bandgap structures) was made to describe those periodic materials [27].

The first experimental research in microstructured fibers proved that light can be guided through a fiber of this type. In 1996 Russell's group [28] reported the first silica fiber with solid core surrounded by air holes in the cladding, a picture of this fiber is shown in Figure 1.3. This invention took place at Southampton University, England. Russell named this fiber as photonic crystal fiber.

The behavior of a PCF is similar to a semiconductor, in both cases a spatially, periodically distributed potential causes the opening of forbidden gaps in the dispersion relations for photon and electron waves [29]. In simpler words, the electronic bandgaps are caused by periodically varying electric potential from the lattice arrangement of the atoms constituting the semiconductor, and a periodic distribution of a dielectric potential causes the bandgaps to open in photonic crystals.

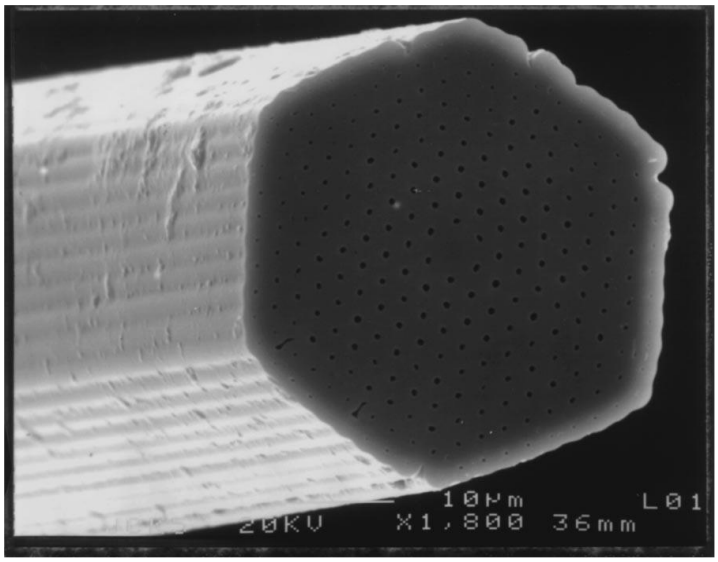

Figure 1.3 Picture of the first PCF reported in 1996 by Russell and company. Courtesy of [28].

An exploited advantage of PCF's is that they have high design flexibility. In particular, by changing the geometric characteristics of the air-holes in the fiber cross section; e. g. PCFs with small core and large air-holes have better nonlinear properties compared with traditional optical fibers. On the contrary, fibers with small air-holes and large hole to hole distances are useful for high power delivery [30].

Some of the disadvantages of PCFs are the difficulty to fabricate them and their high enough losses in comparison with conventional optical fibers.

1.2.1Classes of Photonic Crystal Fibers

There are two main categories of PCFs: high-index guiding fibers and photonic bandgap fibers. The first category is similar to conventional optical fibers, the light travels in a solid core and the cladding has a lattice of air-holes. The light remains in the core due total internal reflection, with a few differences explained in the next section. The second category does not have a solid core; instead it has a complete lattice of air-holes in its entire surface. In this PCF class, the light propagates by a mechanism different from total internal reflection, which is, by exploiting the presence of the photonic bandgap (PBG). In a few words, the PBG creates a region where light in certain wavelength ranges cannot propagate [30].

The high-index core PCFs are classified in three different sub-classes [31, 32, 33]:

- High Numerical Aperture (HNA) fibers.
- Highly Non-Linear (HNL) fibers.
- Large Mode Area (LMA) fibers.

PBG fibers can be also classified in three sub-classes [34, 35]:

- Low-Index Core (LIC) fibers.
- Air-Guiding (AG) or Hollow-Core (HC) fibers.
- Bragg Fiber (BF).

Figure 1.4 shows pictures of the PCF classes and sub-classes. A deeper explanation of each PCF type is presented for Bjarklev *et al.* [31].

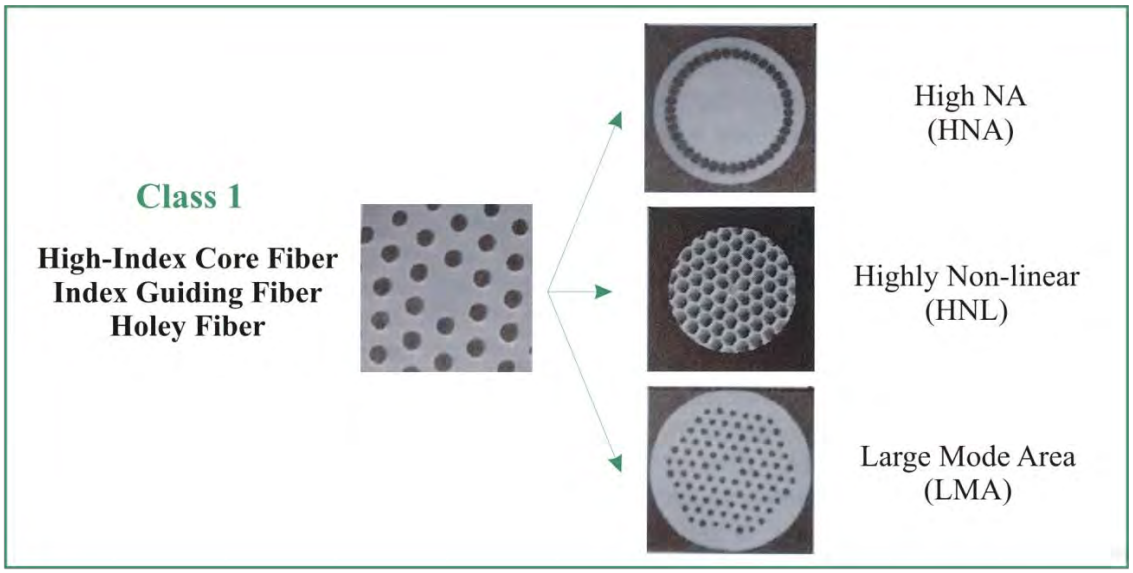

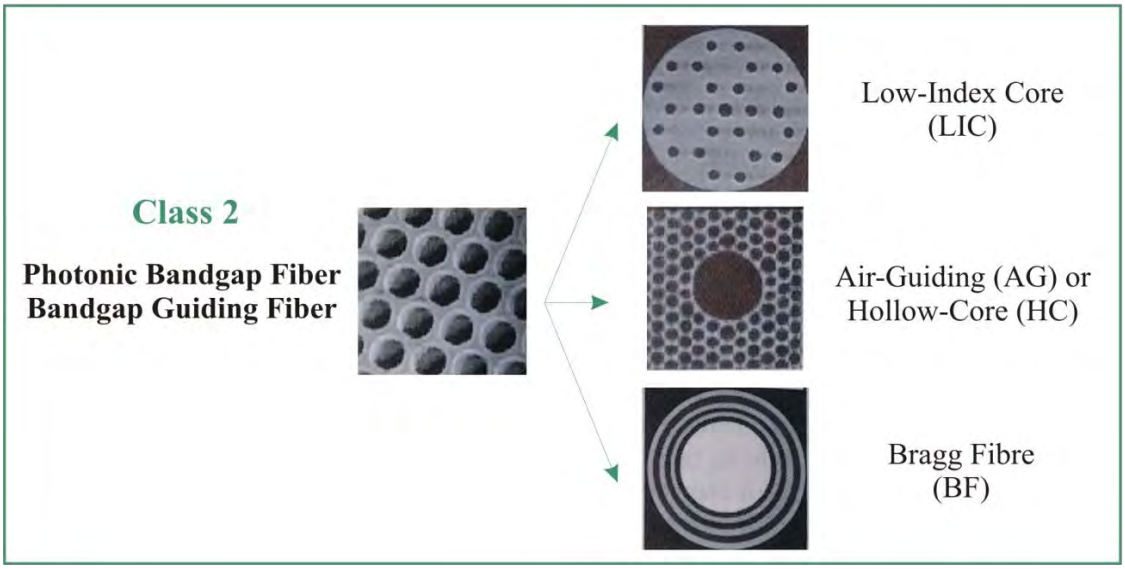

Figure 1.4 Diagram of the main classes and sub-classes of PCFs. Optical fiber pictures courtesy of [31].

In this work, HNL PCFs were used and in the following sections its properties will be studied.

1.2.2Guidance mechanism of High-Index Core PCF

High-Index Core PCF are said to guide light by modified total internal reflection (MTIR) [36]. The idea is to use an equivalent step index fiber model. In this case, the refractive index of the cladding, n_{FSM}, is considered to be lower than the one in the core. A raw idea is to consider n_{FSM} as an average of the refractive index of the air-holes and background area around the core, but a more complex analysis is necessary to valid this model.

The modes in step index fibers are characterized by a propagation constant β, which is the component of the wave vector in the direction of the central fiber axis. The value of this constant will determine if a wave is radially propagative or evanescent in the core and in the cladding. A similar analysis can be done in PCFs, but it is necessary to define two main equivalent regions: the core and the cladding.

Considering a PCF like the one showed in the left side of Figure 1.5, the core region will be delimited for a circle centered on the fiber axis and touching the first set of air-holes; then the cladding will be the outer region.

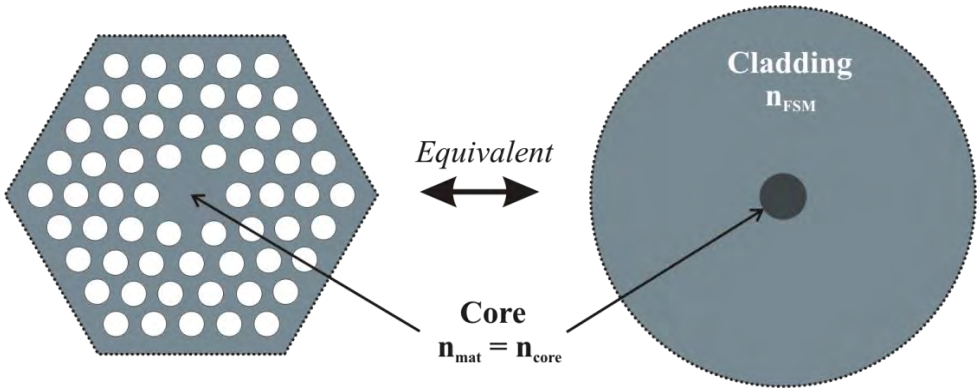

Figure 1.5 Equivalent model of a High-Index Core PCF with a step index fiber.

The core refractive index n_{core} in the equivalent step index model is considered the same one in background material n_{mat}. From step index guidance theory [37], it is known that fields that satisfy Equation (1.3) are propagative in radial direction within the core, otherwise they are evanescent.

$$n_{eff} = \frac{\beta}{k_0} < n_{core} \tag{1.3}$$

In Equation (1.3), k_0 represents the free space wavenumber and n_{eff} .is the effective refractive index of the propagated field.

This approach is valid for the core region in PCFs. In case of the cladding region, Maxwell's equations have to be solved to find out whether fields with a given propagation constant β can exist or not in the photonic crystal [36].

Summarizing, MTIR takes place due an approach based in the replacement of an inhomogeneous structure with a homogenous one. This approach has been proved to be accurate for design applications without heavy and time consuming computations [38].

1.3 Fabrication of PCFs

In fiber optic fabrication, there are two main steps: fabrication of the fiber preform and drawing of this preform using a special structure.

For conventional optical fibers, the preform usually is made with various vapor deposition techniques, which have given a well-established process, obtaining circular-symmetric preforms. With vapor deposition techniques, very low impurities and precisely controlled doping levels are achieved [39].

However, in the case of PCF's, vapor deposition is not a suitable preform fabrication method due to its geometrical structure is more complex and it is not necessary circular or symmetrical. Hence, other preform fabrication methods are required for this technology.

Once the preform is made, a drawing process is performed to reduce its diameter and give it the desired fiber dimensions. In some cases, more than one step drawing is necessary [41].

1.3.1PCF preform fabrication

Nowadays there are several methods for the fabrication of PCF preforms; some of them are: drilling, extrusion, casting and stacking [40]. Each method is ideal for a specific type of PCF.

1.3.1.1 Drilling

This method is used for microstructured polymer optical fibers (MPOF), where complex preform structures can be achieved using a computer numerical control (CNC) mill. The obtained performs are usually short and thick, the longest preform reported was 140 mm [42]. Figure 1.6 shows a CNC mill drilling a polymer bulk to create a MPOF preform.

Using this technique, air-holes collapse is expected during fabrication, around 30-40% [42].

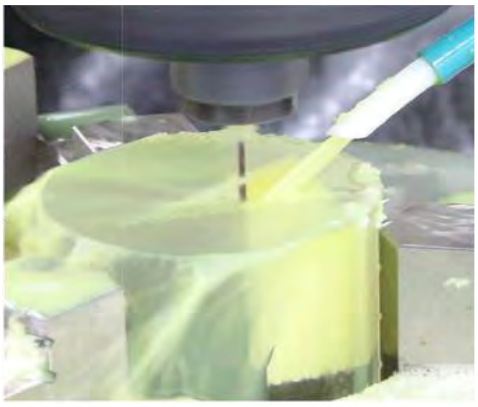

Figure 1.6 CNC mill drilling a primary MPOF preform. Courtesy of [40].

1.3.1.2 Extrusion

This technique is particularly suitable for making glass preforms based on soft glasses and polymers. The process consists in creating a heated bulk material and force it under high pressure through a die containing a pattern with the required preform transverse structure [43].

A benefit of extrusion technique is that lower losses are possible since fewer surfaces are in contact with the preform, so the fiber will have fewer impurities.

1.3.1.3 Casting

A mould containing an array of mandrel elements is assembled and then filled with colloidal silica dispersed at high pH, and then the pH is lowered causing the sol to gel. Now it is possible to remove the mandrel elements, leaving air columns within the gel body. After a chemical treatment, the dried porous gel body is then sintered near 1600 ^{o}C into viscous glass [44].

1.3.1.4 Stacking

This technique is generally used for all types of material in the fabrication of PCF preforms. These preforms are made by stacking capillaries and rods in a specific arrangement and inserting the stack in a larger tube prior drawing. Using this technique allows to fabricate PCF with triangular or square lattice structures with simple radial geometry structure [45]. Figure 1.7 shows a special

structure where capillaries and rods are placed in the desired position, depending in the PCF design.

Figure 1.7 Structure for placing capillaries and rods for manufacturing a PCF preform. Courtesy of [46].

1.3.2PCF drawing process

The preform now is drawing in a special structure called drawing tower. There, it goes through a furnace where is melted at about 2000 ºC (Figure 1.5), and it is feed at a relative low speed (in mm/min). At the beginning of the fusion process, a glass drop is created due gravity force and it is pulled down until a thin thread is formed. The resulted thread continues being pulled down at higher speed (in m/min) to reduce its diameter. A diameter monitor is scanning the current fiber diameter; it consists in a set of precision cameras placed in different axis direction to ensure a consistent diameter along the fiber.

Then, it passes through a container which has the polymer coating die, and after that the fiber goes through the UV curing system; that is a group of ultraviolet lamp in a special refrigerated structure. The complete drawing process is displayed in Figure 1.6.

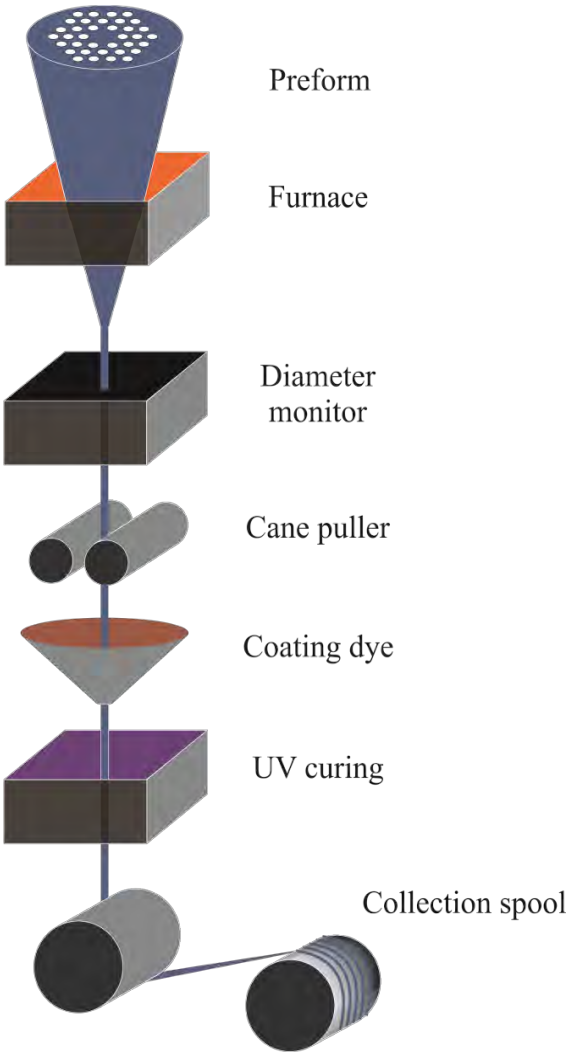

Figure 1.6 PCF drawing process.

1.4 Characteristics of Highly Non-linear PCFs

HNL PCFs have been widely used in the last years due their high non-linear properties. Their high non-linear coefficient and designable properties (see next section) make them suitable for applications in spectroscopy, sensors, telecommunications and supercontinuum generation. Among these applications, supercontinuum generation is the most intensively investigated [47-49].

The most attractive characteristic of HNL PCF is that with relative low optical powers it is possible to induce significant non-linear effects. To measure this feature, the effective nonlinearity γ is used [50], given by:

$$\gamma = \frac{2\pi n_2}{\lambda A_{eff}} \tag{1.4}$$

Where n_2 is the nonlinear coefficient of the material ($n_2 \approx 2.2x10^{-20} m^2/W$ for pure silica), A_{eff} is the effective mode area (discussed in the next chapter) and λ is the free space optical wavelength.

As a comparison, conventional telecommunication optical fiber (such as SMF28) has a non-linear coefficient of $\gamma \approx 1\, W^{-1}km^{-1}$, while for HNL PCF's values of $\gamma \approx 52\ W^{-1}km^{-1}$ have been reported [51].

However, HNL PCFs have higher losses, mainly because their small core. This feature produces an increase in the confinement losses, which can be understood as the losses due the leak of the propagating mode into the cladding when the core diameter is as small as the light wavelength. These losses can be reduced in two ways: increasing the hole to hole distance or increasing the number of hole rings around the core [52].

Moreover, its fabrication requires a two-step drawing when stack and draw technique is used. The first step is to place all the capillaries and rods in the desired position, and then it is covered with a jacket. The structure is drawing to obtain a thinner cane, and finally another jacket is placed to give the typical HNL PCF geometry. Figure 1.7 shows this process.

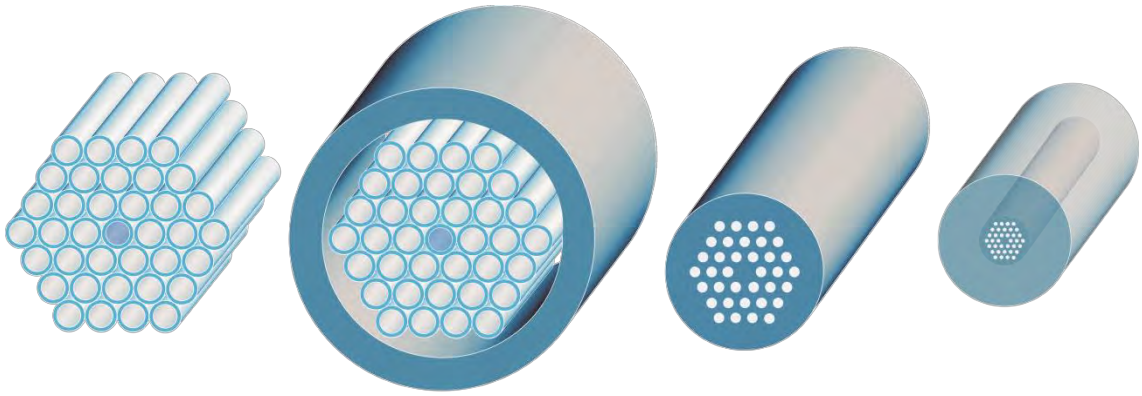

Figure 1.7 Overview of HNL PCFs preforms fabrication: a) stacking capillaries and rods, b) placing a jacket, c) drawing the structure to have a thinner cane and d) placing another jacket to obtain the desired cross section geometry.

The stack and draw technique is used at CIO to fabricate HNL PCFs. Figure 1.8 displays the cross section of a HNL PCF made at CIO.

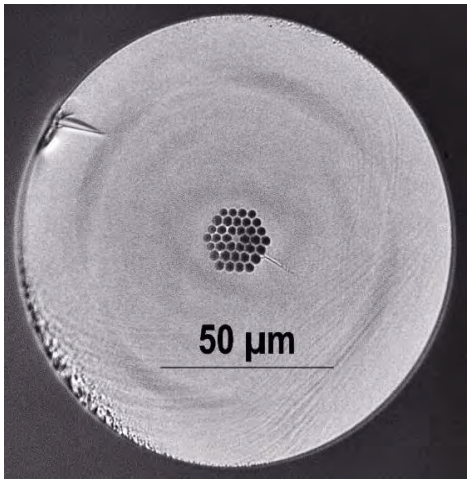

Figure 1.8 Microscope picture of a HNL PCF cross section fabricated at CIO.

Chapter 2
Design and fabrication of HNL IG PCFs

There are several numerical models for PCFs, such as the plane wave expansion method [53], the multipole method [54], the finite element method (FEM) [55, 56], and so on. However, those numerical models are time consuming and costly. Koshiba and Saitoh [57] have proposed an alternative method based on the V (normalized frequency) and W (normalized transverse attenuation constant) parameters.

In this model, it is possible to simple design a PCF considering only wavelengths and structural parameters. The structural parameters of a PCF are the air hole diameter d and the hole to hole distance or pitch Λ, as shown in Figure 2.1.

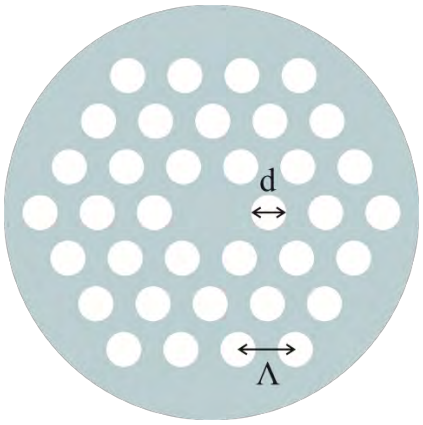

Figure 2.1 Structural parameters of a PCF: air hole diameter d and hole to hole distance or pitch Λ.

The accuracy of the proposed model is high and it can be compared with more complex models, such as FEM, but it is not necessary to use heavy numerical computations.

2.1 The V parameter expression

The V parameter (normalized frequency) has been used in the design of conventional optical fibers; its expression is given by:

$$V = \frac{2\pi}{\lambda} a\sqrt{n_{co}^2 - n_{cl}^2} = \sqrt{U^2 + W^2} \tag{2.1}$$

Where

$$U = \frac{2\pi}{\lambda} a\sqrt{n_{co}^2 - n_{eff}^2} \tag{2.2}$$

$$W = \frac{2\pi}{\lambda} a\sqrt{n_{eff}^2 - n_{cl}^2} \tag{2.3}$$

where λ is the operating wavelength a is the core radius, n_{co} is the core index, n_{cl} is the cladding index, and n_{eff} is the effective index of the fundamental guided mode. Parameters U and W are called the normalized transverse phase and attenuation constants respectively.

Considering a PCF with a triangular lattice of holes where d is the hole diameter and Λ is the pitch, Mortensen *et al* [58] proposed the following effective V parameters:

$$V_{eff} = \frac{2\pi}{\lambda}\Lambda\sqrt{n_{eff}^2 - n_{FSM}^2} \tag{2.4}$$

Where n_{FSM} is the effective cladding index, defined as the effective index of the so-called fundamental space-filling modeling the triangular air-hole lattice [58]. However, this definition is intrinsically different from the original Equation (2.1); therefore heavy numerical computations are necessary to calculate the values of n_{eff}.

Koshiba and Saitoh introduced the effective V parameter shown in Equation (2.5), where a_{eff} is the effective core radius that is assumed to be $\Lambda/\sqrt{3}$ [57]. They compared several V values calculated through vector FEM as a function of λ/Λ for different d/Λ values and by trial and error; they found that each value can be fitted to a function of the form exposed in Equation (2.6).

$$V_{eff} = \frac{2\pi}{\lambda}a_{eff}\sqrt{n_{co}^2 - n_{FSM}^2} \tag{2.5}$$

$$V\left(\frac{\lambda}{\Lambda}, \frac{d}{\Lambda}\right) = A_1 + \frac{A_2}{1 + A_3 \exp\left(A_4 \frac{\lambda}{\Lambda}\right)} \tag{2.6}$$

The fitting parameters A in Equation (2.6) depend on d/Λ only, and they are well described by the following expression:

$$A_i = a_{i0} + a_{i1}\left(\frac{d}{\Lambda}\right)^{b_{i1}} + a_{i2}\left(\frac{d}{\Lambda}\right)^{b_{i2}} + a_{i3}\left(\frac{d}{\Lambda}\right)^{b_{i3}} \tag{2.7}$$

and the coefficients a and b are given in Table 2.1.

	i=1	*i=2*	*i=3*	*i=4*
a_{i0}	0.54808	0.71041	0.16904	–1.52736
a_{i1}	5.00401	9.73491	1.85765	1.06745
a_{i2}	–10.43248	47.41496	18.966849	1.93229
a_{i3}	8.22992	–437.50962	–42.4318	3.89
b_{i1}	5	1.80	1.7	–0.84

b_{i2}	7	7.32	10.0	1.02
b_{i3}	9	22.80	14.0	13.40

Table 2.1 Fitting coefficients for Equation (2.7).

With the effective V parameter described in Equation (2.6), it is possible to obtain the n_{FSM} without the need for numerical computations. Koshiba and Saitoh reports that using this equation gives values of n_{FSM} , which deviates less than 0.25% from the values obtained through vector FEM for $\lambda/\Lambda < 1.5$ and V > 0.85.

Figure 2.2 shows the effective V parameter as function of λ/Λ. Using Equations (2.5) and (2.6) it was possible to obtain the value of n_{FSM} as a function of λ/Λ, as it is shown in Figure 3.3.

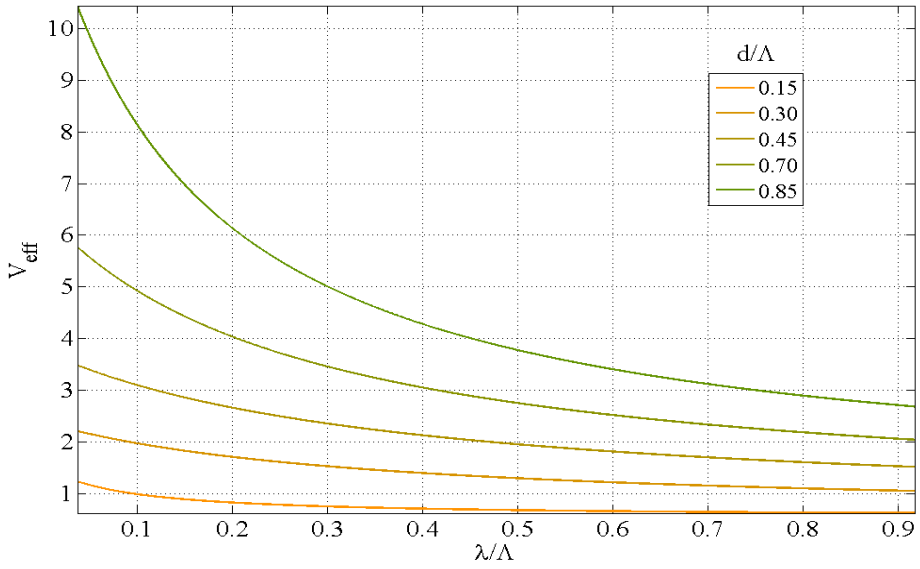

Figure 2.1 Effective V parameter as function of λ/Λ.

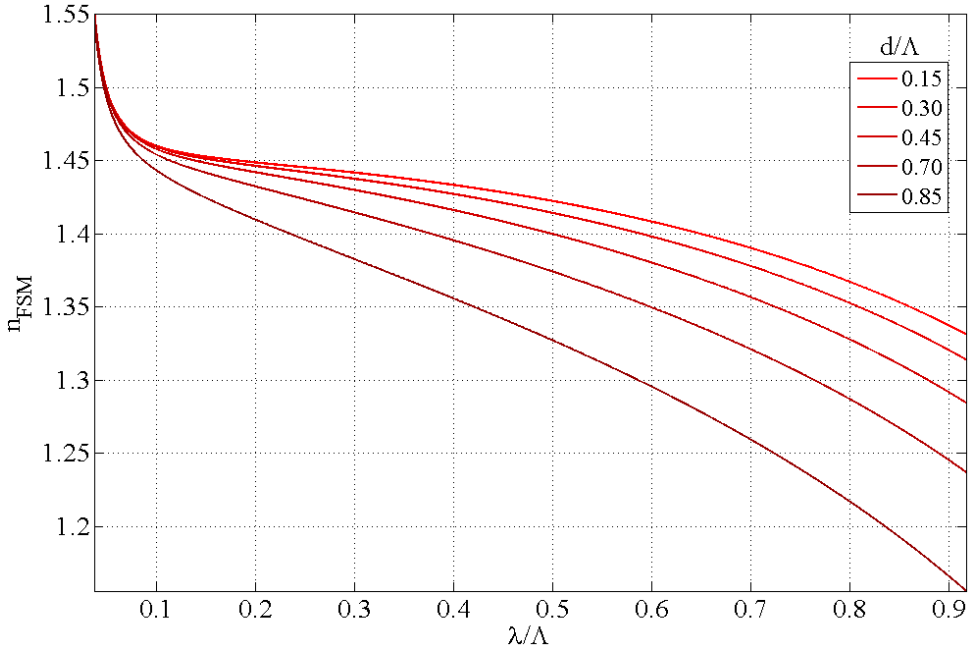

Figure 2.2 Effective cladding index n_{FSM} as a function of λ/Λ.

2.2 The W parameter expression

Using the V parameter it is easy to obtain the effective cladding index n_{FSM}, however, it is usually needed heavy numerical computations to obtain accurate values of n_{eff}. It would be more convenient to have an empirical relation for the W parameter [57].

Saitoh and Koshiba calculated W values through vector FEM as a function of λ/Λ for different d/Λ values. Then, by trial and error they found that each data could be fitted to the same function in Equation (2.9) as:

$$W\left(\frac{\lambda}{\Lambda},\frac{d}{\Lambda}\right)=B_1+\frac{B_2}{1+B_3\exp\left(B_4\frac{\lambda}{\Lambda}\right)} \tag{2.8}$$

the fitting parameters B depend on d/Λ only, and they are well described by the following expression:

$$B_i=c_{i0}+c_{i1}\left(\frac{d}{\Lambda}\right)^{d_{i1}}+c_{i2}\left(\frac{d}{\Lambda}\right)^{d_{i2}}+c_{i3}\left(\frac{d}{\Lambda}\right)^{d_{i3}} \tag{2.9}$$

and the coefficients c and d are given in Table 2.2.

	i=1	*i=2*	*i=3*	*i=4*
c_{i0}	–0.0973	0.53193	0.24876	5.29801
c_{i1}	–16.70566	6.70858	2.72423	0.05142
c_{i2}	67.13845	52.04855	13.28649	–5.18302
c_{i3}	–50.25518	–540.66947	–36.80372	2.7641
d_{i1}	7	1.49	3.85	–2
d_{i2}	9	6.58	10	0.41
d_{i3}	10	24.8	15	6

Table 2.2 Fitting coefficients for Equation (2.10).

Figure 2.3 shows the effective W parameter as function of λ/Λ for different values of d/Λ.

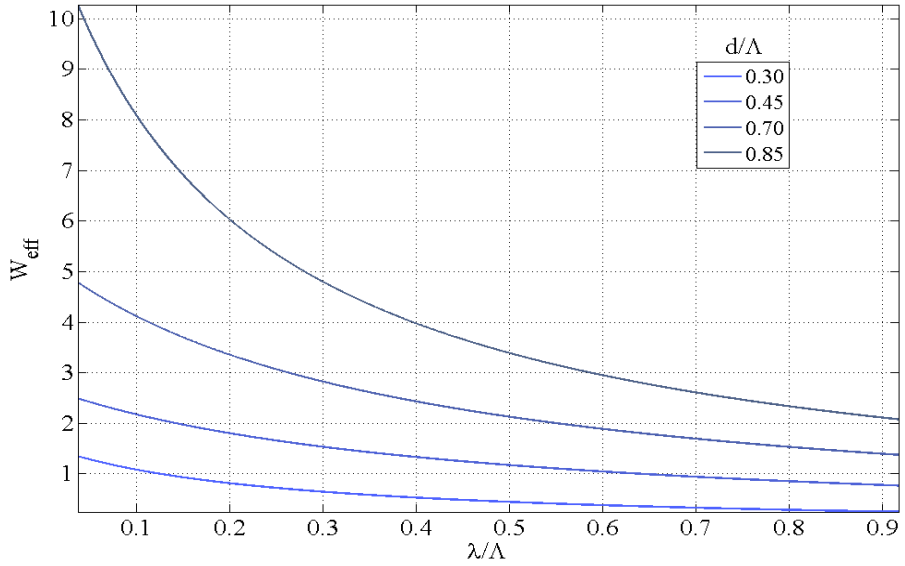

Figure 2.3 Effective W parameter as function of λ/Λ.

Using Equations (2.3) and (2.9) gives the n_{eff} as a function of λ/Λ, as seen in Figure 2.4. With $\lambda/\Lambda \leq 1.5$ and $W \geq 0.1$, these equations have a maximum error of 0.15 %, compared with FEM method.

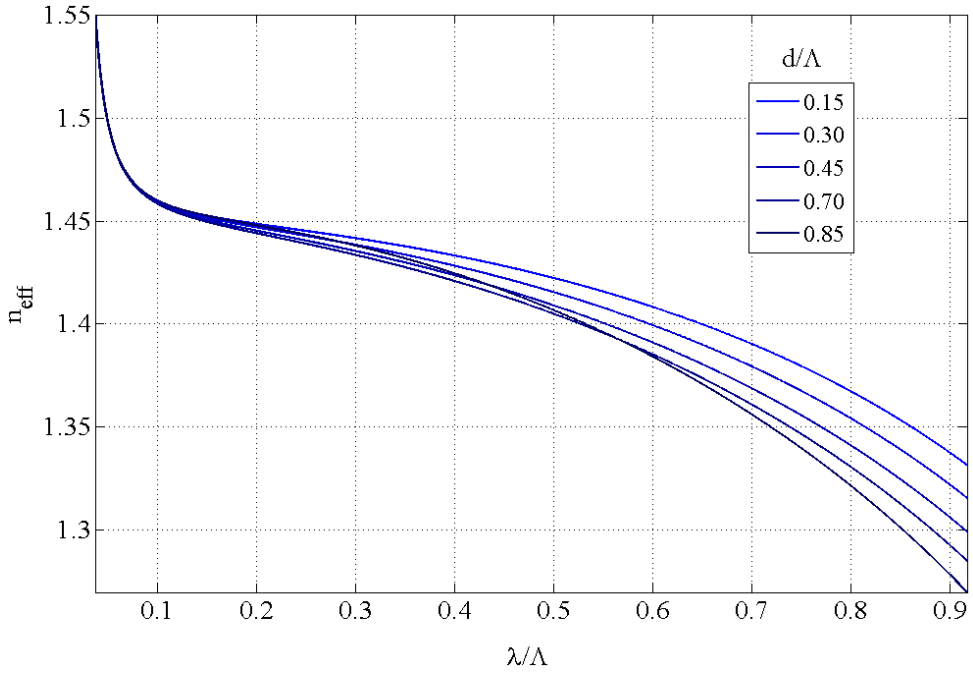

Figure 2.4 Effective index n_{eff} as function of λ/Λ.

Since a step index model is considered, it is possible to determine if a PCF is single-mode or multimode. From Equations (2.5), (2.6) and considering the cutoff condition $V_{eff} = 2.405$ [60], regions of single-mode and multimode can be determined, depending in the geometrical PCF parameters. When the ratio d/Λ is lower than 0.4, the PCF will have an endlessly single-mode behavior, regardless the light wavelength, as shown in Figure 2.5.

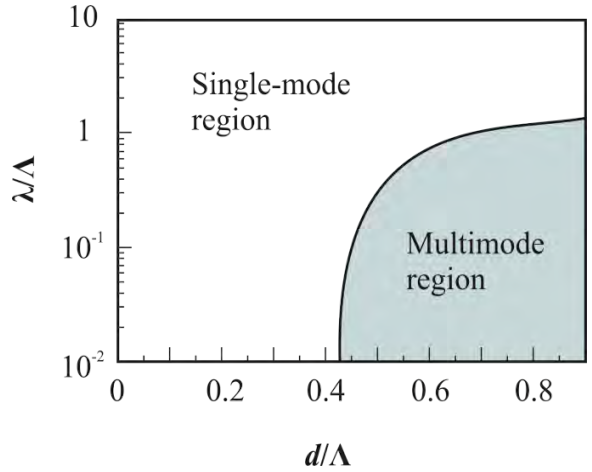

Figure 2.5 Modal behavior of a PCF depending on its geometrical parameters.

2.3 Computing PCF features

2.3.1Dispersion

With the previous equations, it is relatively easy to find the effective refractive index of a PCF. We can use this value to compute the dispersion in the fiber. Assuming that the waveguide's contribution to dispersion parameter D is independent of material dispersion D_m, dispersion can be estimated as:

$$D = -\frac{\lambda}{c}\frac{d^2 n_{eff}}{d\lambda^2} + D_m \tag{2.10}$$

Where c is the light speed in vacuum and D_m is determined by Sellmeier relation [61]:

$$n^2(\lambda) = 1 + \frac{B_1\lambda^2}{\lambda^2 - C_1} + \frac{B_2\lambda^2}{\lambda^2 - C_2} + \frac{B_3\lambda^2}{\lambda^2 - C_3} \tag{2.11}$$

Where B_i and C_i are coefficients with values for fused silica are shown in Table 2.3

B_1 (µm)	B_2 (µm)	B_3 (µm)	C_1 (µm^2)	C_2 (µm^2)	C_3 (µm^2)
0.6961663	0.4079426	0.8974794	4.679148×10−3	1.351206×10−2	97.93400

Table 2.3 Sellmeier coefficients for fused silica [61].

Notice that the second term in Equation (2.10) is not directly calculated. In order to consider it, Equation (2.11) is used in every computation in this chapter.

2.3.2Mode field diameter

Mode field diameter (MFD) can be evaluated using the Marcouse formula [59]:

$$\frac{w_{eff}}{a_{eff}} = 0.65 + \frac{1.619}{V_{eff}^{3/2}} + \frac{2.879}{V_{eff}^{6}} \tag{2.12}$$

where w_{eff} is the half-MFD and is called the effective modal spot size.

2.3.3Beam divergence

Gaussian-beam-propagation theory states that beam divergence θ is given by [60]:

$$\theta = \tan^{-1}\left(\frac{\lambda}{\pi w_{eff}}\right) \tag{2.13}$$

This value indicates how fast the light beam expands when it exits the optical fiber.

The recently explained method provides an acceptable approach to design PCFs with relative simple computations. In next chapter, a set of seven HNL PCFs is characterized.

2.4 HNL IG PCF fabrication

Fabrication of HNL IG PCF is a complicated process and takes a lot of time. At the first time we calculated design of the first preform. On a base of results obtained in [63], we designed a preform with 3 rings of air holes in a PCF cladding. Limited number of air-holes in the cladding give possibility to simplify greatly a problem of HNL IG PCF fabrication. For this type of a preform, it is necessary of about three weeks to draw (for one preform) needed capillaries with outside diameters of 1.93±0.005 mm, solid packers of different diameters and a solid core rod (usually two of them) with an outside diameter of 1.93±0.005 mm. Then the fabricated capillaries are arranged carefully in a hexagonal structure around the core rod giving a stack. Solid packers are included at the edge of the stack to prevent distortion of the stack at the inserting of it into a jacketing tube with inside diameter of 16 mm and outside diameter of 20 mm. It is necessary of about two weeks to do it. The stack design is shown in figure 2.6 (a). The stack was drawn into 5 canes with outside diameters of 1.8±0.05 mm. An optical microscope image of a cane cross section is shown in figure 2.6 (b).

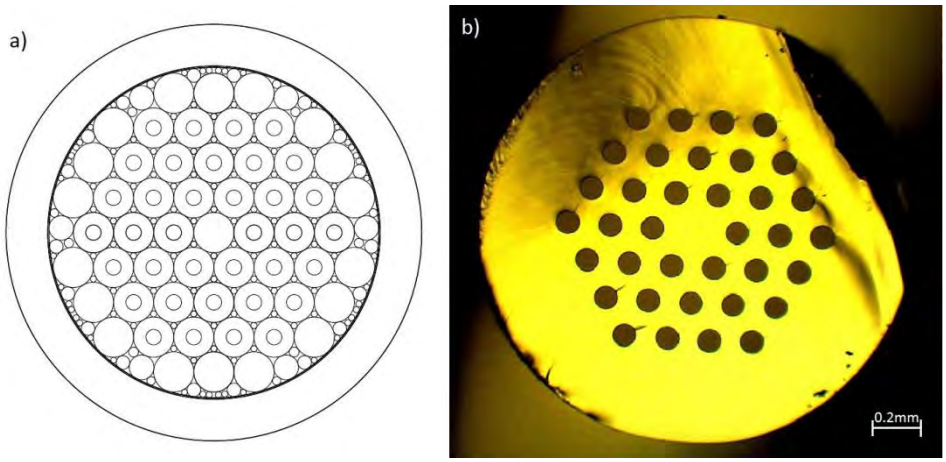

Figure 2.6. a) Stack design photo of fabricated preform with 3 rings of air holes, b) optical microscope image of a fabricated cane cross section.

Average diameter of the holes d in the canes is 104 µm, average dimension of the pitch Λ is 179 µm. To draw a fiber, canes was inserted into a jacketing tube with 1.85 mm inside diameter (ID) and 12 mm outside diameter (OD). During the draw a pressure is applied to the holes. The draw rate was set to give a fiber OD of 123.5±0.5 µm, the temperature was 1950°C. The optical microscope images of two fabricated fiber cross sections are shown in figure 2.7.

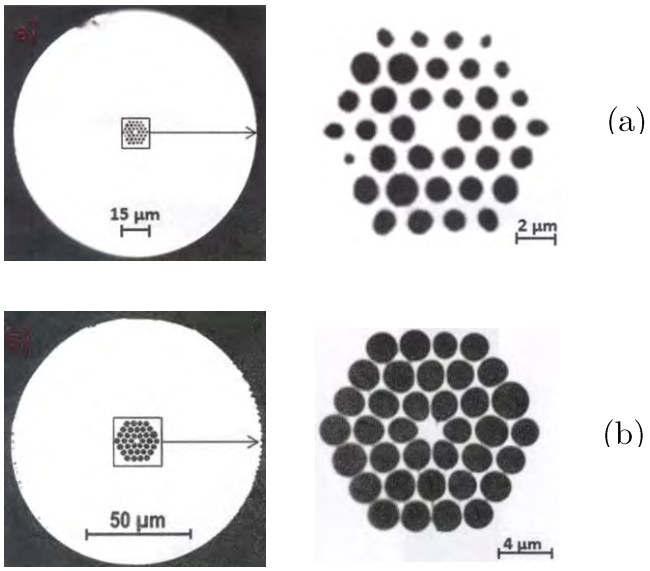

Figure 2.7. Optical microscope images of two fabricated fiber cross section: a) 3.6(100), b) 4.0(108).

Pressures into holes for fiber 3.6(100) was 100 mBar, for 4.0(108) – 108 mBar. The optical microscope images of the next 3 fabricated fiber cross sections are shown in Figure 2.8.

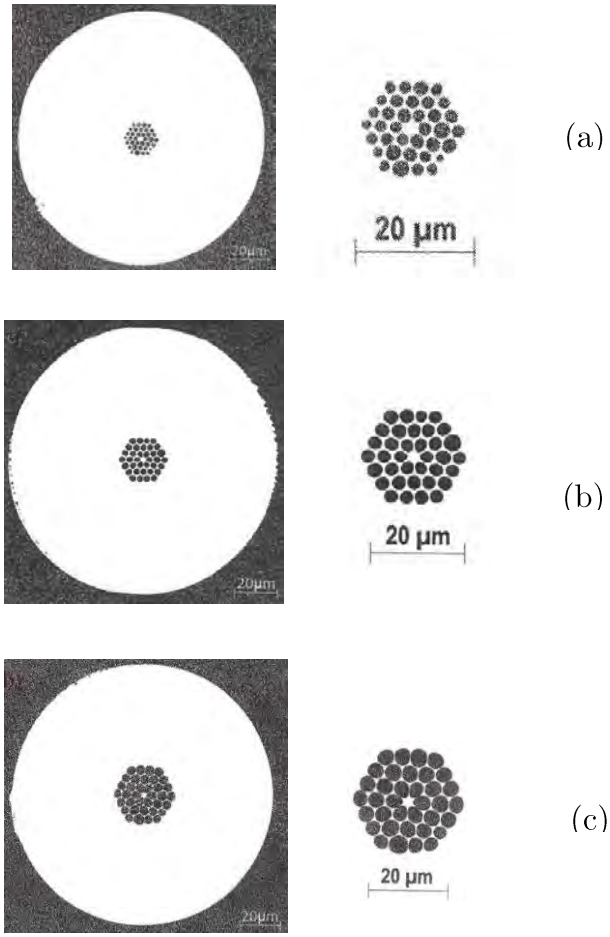

Figure 2.8. Optical microscope images of next three fabricated fiber cross section: a) 3.2(100), b) 4.0(115), c) 2.5(100).

Pressures into holes for fiber 3.2(100) was 100 mBar, for 4.0(115) – 115 mBar, for 2.5(100) – 100 mBar. To decrease possible attenuation in fabricated HNL IG PCFs we designed a preform with 6 rings of air holes in their cladding. Unfortunately, fabrication of such PCFs is more complicated process than fabrication of PCFs with limited number of air holes in the cladding. The stack design is shown in Figure 2.9 (a). For this type of preform it is necessary to draw about 140 capillaries with outside diameters of 1.66±0.005 mm, solid packers of different diameters and a solid core rod (usually two of them) with an outside diameter of 1.66±0.005 mm. Then the fabricated capillaries are arranged in a hexagonal structure around the core rod giving a shack. Many solid packers are included at the edge of the stack to prevent distortion of the stack at the

inserting of it into a jacketing tube. Figure 2.8(b) and 2.8(c) show stacking result of obtained capillaries and packers. The Stack was drawn then into five canes with outside diameters of 3.0±0.05 mm. Figure 2.8(d) shows a photo of optical microscope image of a fabricated cane cross section.

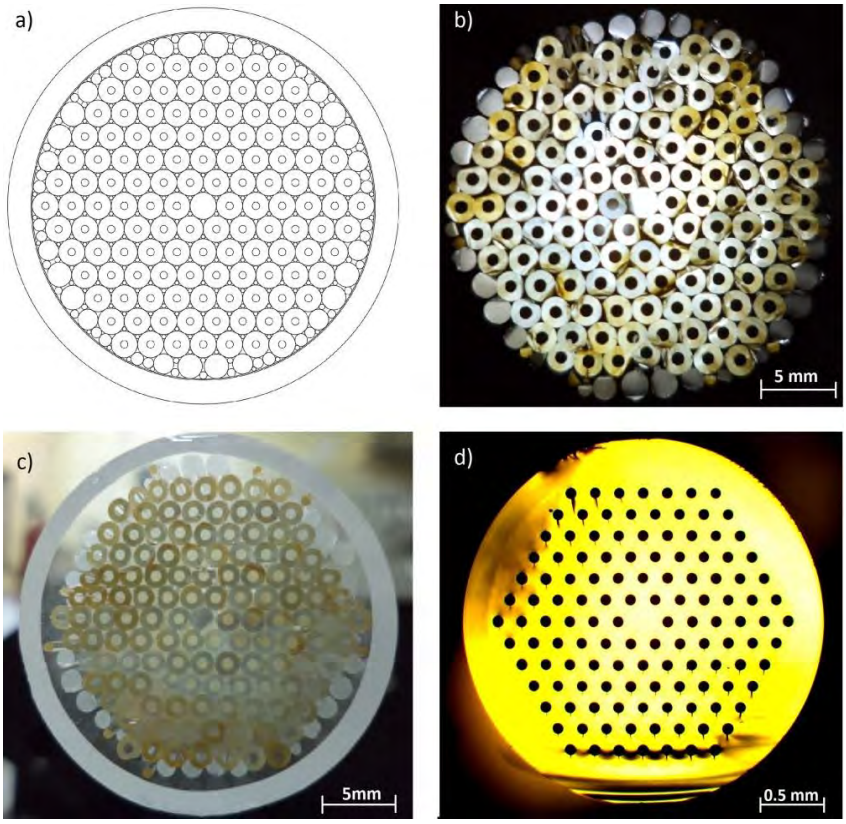

Figure 2.8. (a) Design of a stack for a PCF with 6 ring of air holes in the cladding, (b) and (c) fabricated stack of capillaries and packers, (d) photo of an optical microscope image for a fabricated cane cross section.

Average diameter d of the holes in the cane is 76 µm, average value of the pitch Λ is 182 µm. Using the fabricated canes, about 6 different fibers with different parameters of pressure, temperature, draw velocity were fabricated. The draw rate was set to obtain a fiber outside diameter of 123.5±0.5 µm. A photo of an optical microscope image for an 8.0(1900) fabricated fiber cross section is shown in figure 2.9(a). The fiber was drawn at a pressure inside holes of 115 mBar and a drawing velocity of 35 m/min. For comparison, a photo of an experimental HNL IG PCFs with a core doped with germanium (Ge), manufactured in Central Glass & Ceramic Research Institute, Calcutta, India is shown in figure 2.9(b). Measurement of geometric parameters and characterization of the mentioned earlier HNL IG PCFs will be conducted in the next chapter.

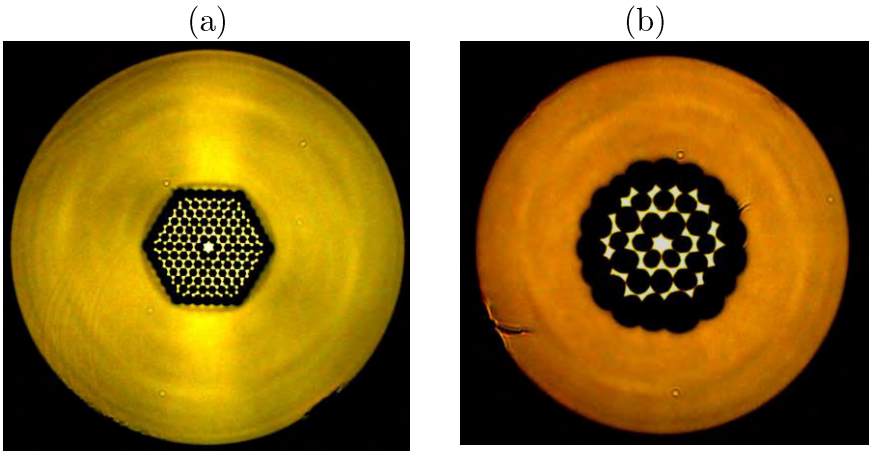

Figure 2.9. Optical microscope images of two fiber cross section: a) 8.0(1900) PCF, b) HNL IG PCFs with a core doped with germanium.

Chapter 3
HNL IG PCF measurement, analysis and results

Once the design and fabrication of PCFs are done, the next step is to characterize them. Using the theoretical model explained in Chapter 2, for each PCF it is possible to obtain the refractive index of the core and cladding, its dispersion curve and beam divergence. However, those parameters are not enough to provide a good fiber description; two more characteristicsc are indispensable to report: losses and numerical aperture.

Seven all silica HNL PCFs were characterized in this work; six of them were made in CIO, and those fibers were named as: *3.6(100)*, *4.0(108)*, *3.2(100)*, *4.0(115)*, *2.5(100)* and *8.0(1900)*. The seventh HNL PCF was kindly provided by Central Glass & Ceramic Research Institute, Calcutta, India.

The core of this fiber was doped with germanium, reason why it was named as *Ge-doped*.

In order to characterize them, it is necessary to know their geometrical parameters (air hole diameter d and the hole to hole distance or pitch Λ). Table 3.1 shows the geometrical parameters of the six fibers made at CIO.

Fiber	d (µm)	Λ (µm)	d/Λ
2.5(100)	3.63	4.22	0.8602
3.6(100)	1.13	2.03	0.5567
4.0(108)	1.91	2.42	0.7893
3.2(100)	1.74	2.50	0.6960
4.0(115)	2.47	2.86	0.8636
8.0(1900)	2.01	3.18	0.6321

Table 3.1 Geometrical parameters of HNL PCFs fabricated at CIO, measured from atomic force microscope images.

We report two different characterizations for these fibers: one theoretical based on the method explained in Chapter 2 and another experimental for selected fiber features.

3.1 Theoretical characterization

The used approach for PCFs requires their geometrical parameters dimensions, and more specifically the d/Λ ratio. The last column in Table 3.1 displays this ratio for the fibers characterized next.

3.1.1Effective cladding index

To obtain the effective refractive index n_{FSM} behavior in function of λ/Λ, Equations (2.5) and (2.6) were used. We did a MATLAB program to obtain Figure 3.1, which shows n_{FSM} for the studied fibers.

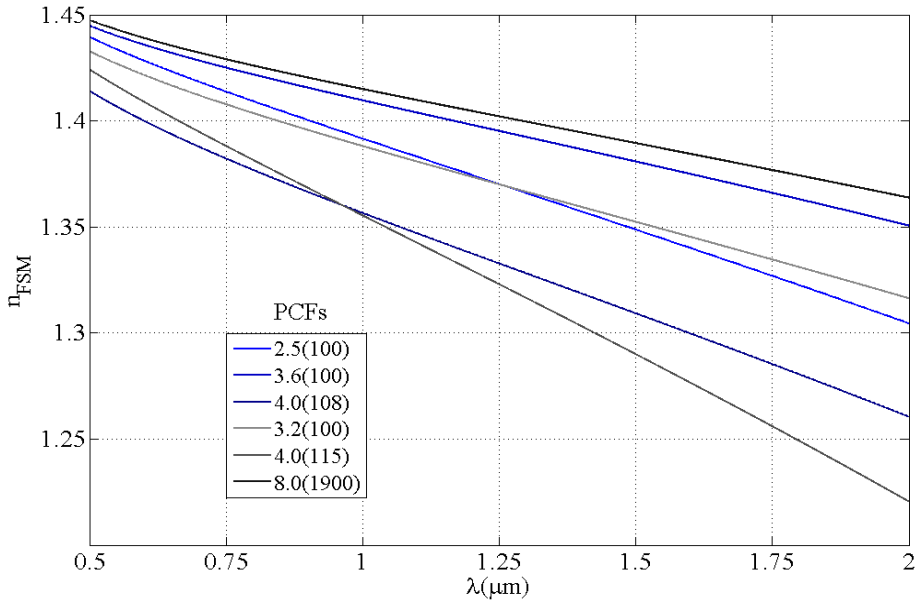

Figure 3.2 Effective cladding index n_{FSM} as a function of λ for 2.5(100), 3.6(100), 4.0(108), 3.2(100), 4.0(115) and 8.0(1900) fibers.

The n_{FSM} has a similar behavior for each fiber, and its theoretical operational range is from 1.45 to 1.25, depending in λ.

3.1.2Effective refractive index

Once the n_{FSM} has been computed, it is possible to obtain the effective refractive index n_{eff} from Equations (2.4) and (2.5). This result is showed in Figure 3.3.

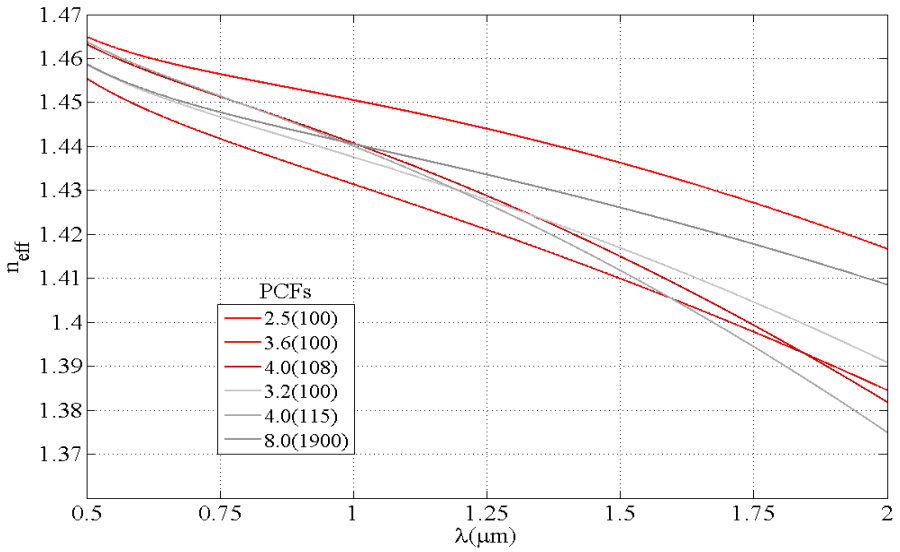

Figure 3.3 Effective refractive index n_{eff} as a function of λ for 2.5(100), 3.6(100), 4.0(108), 3.2(100), 4.0(115) and 8.0(1900) fibers.

It can be seen that for each value of n_{eff} corresponds a lower value for n_{FSM}, then the step index model we are using is valid.

3.1.3Dispersion

With the recently evaluated n_{FSM}, Equation (2.10) was used to plot the characteristic dispersion curve for each fiber, as shown in Figure 3.4.

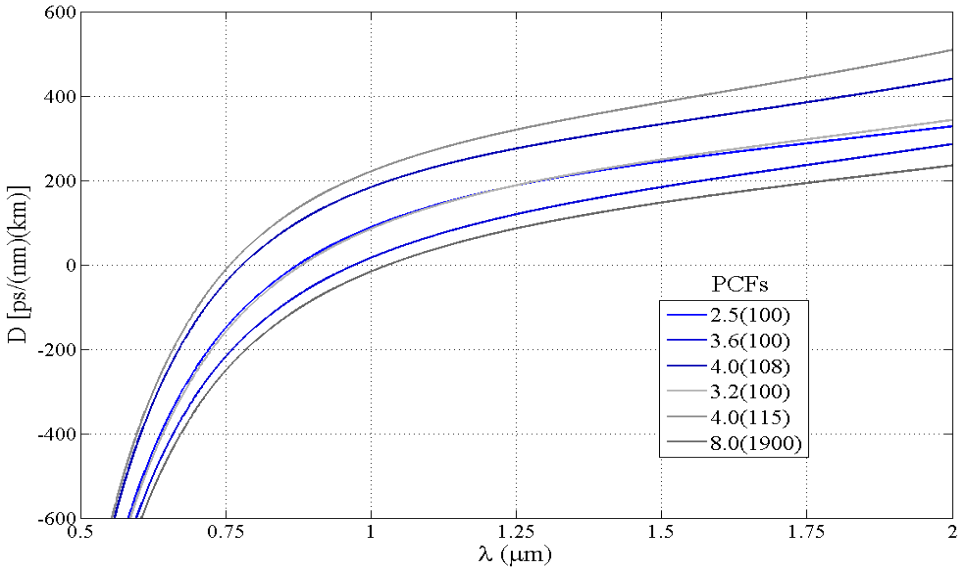

Figure 3.4 Dispersion curves for 2.5(100), 3.6(100), 4.0(108), 3.2(100), 4.0(115) and 8.0(1900) fibers.

As can be seen, for each fiber there is a specific wavelength in which the dispersion value is zero. This wavelength is called zero dispersion wavelength (ZDW). Table 3.2 summarizes the ZDWs for each analyzed fiber.

Fiber	Zero dispersion wavelength (nm)
2.5(100)	874
3.6(100)	971
4.0(108)	779
3.2(100)	881
4.0(115)	758
8.0(1900)	1029

Table 3.2 ZDWs for different fibers, computed using Equation (2.10).

3.1.4Mode field diameter

Using Marcouse formula (Equation 2.10) and considering $a_{eff} = \Lambda/\sqrt{3}$, the MFD can be computed, as shown in Figure 3.5.

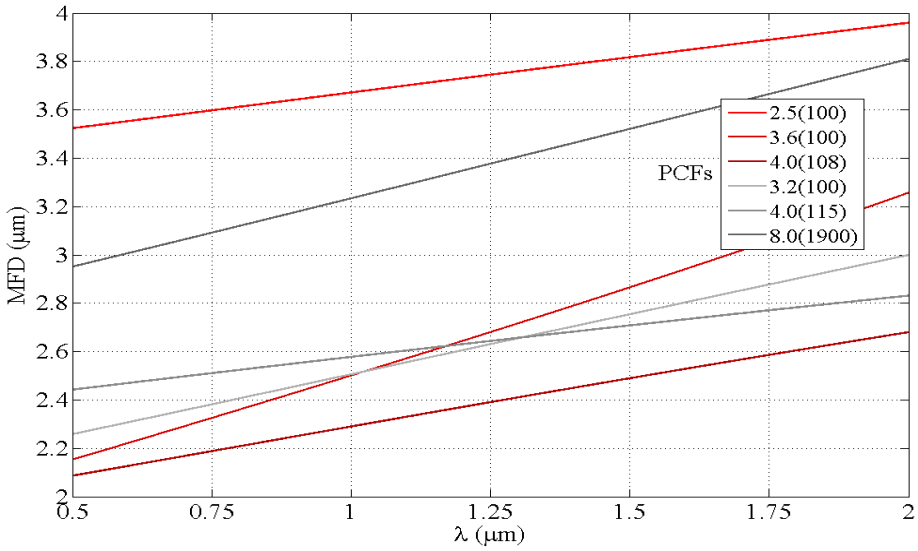

Figure 3.5 MFD as function of λ for 2.5(100), 3.6(100), 4.0(108), 3.2(100), 4.0(115) and 8.0(1900) fibers.

It is important to point out that this MFD is valid only when fundamental mode is propagating in the fiber. To ensure this behavior, Figure 2.5 is useful.

3.1.5Beam divergence

Again, when fundamental mode is propagating, it is possible to compute the beam divergence θ using Equations (2.5) and (2.13). In Figure 3.6, θ is shown for the studied fibers.

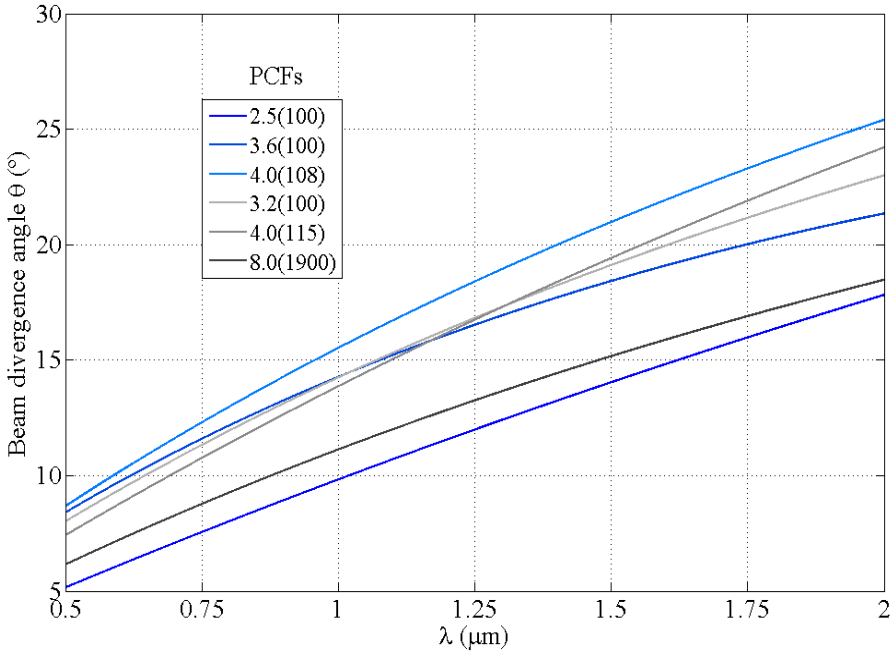

Figure 3.6 Beam divergence θ for 2.5(100), 3.6(100), 4.0(108), 3.2(100), 4.0(115) and 8.0(1900) fibers.

3.2 Experimental setups and results

3.2.1Attenuation

A critical feature of any optical fiber is the attenuation (or transmission losses). It is usually measured in dB/km, and represents the power loss along the optical fiber length. To measure the attenuation of the studied PCFs, an experimental setup shown in Figure 3.7 was used.

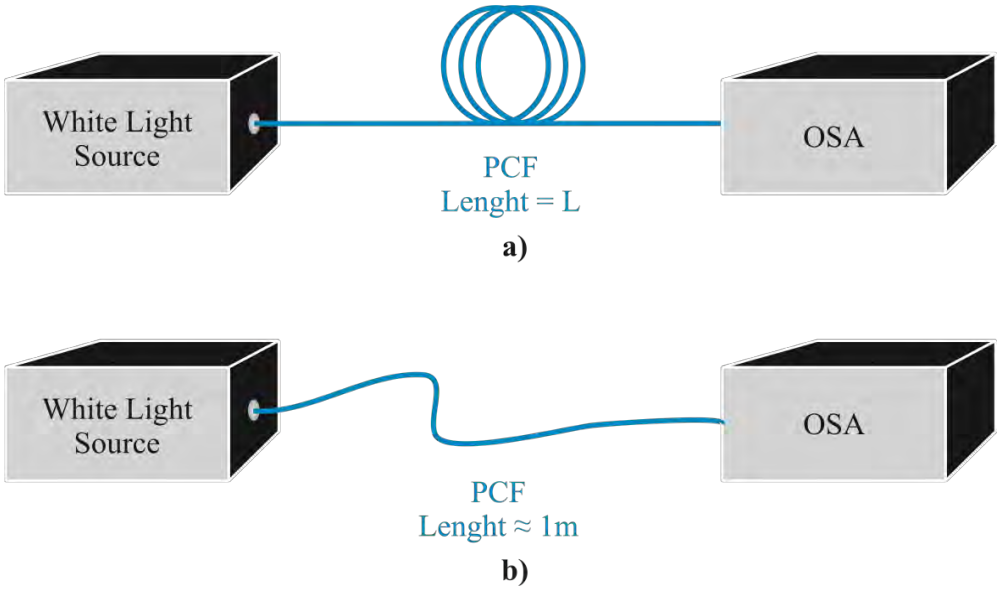

Figure 3.7 Experimental setup for measuring losses in PCFs.

First we connected a PCF with a length L to a white light source, and then we fixed this fiber end to ensure a constant light coupling (Figure 3.7a). The other end was connected to an optical spectrum analyzer (OSA) and we saved its transmission spectra. We repeated three times this step, cleaning and cleaving the fiber end connected to the OSA. This was made to choose the best transmission spectrum among the three measurements performed.

Then, we measured and cut one meter of PCF starting from the white light source, without disconnecting the fiber. We connected the recently created fiber end to the OSA and we measured again three transmission spectra to choose the best of them, like in the previous step (Figure 3.7b).

Once we had both transmissions spectra, we used the following expression to compute the attenuation α:

$$\alpha_{dB/km} = \frac{P_1 - P_2}{L_1 - L_2} \tag{3.11}$$

where P_1 and P_2 are the transmission spectra powers in dBm, for lengths L_1 and L_2, respectively. Notice that the lengths used in Equation (3.1) have to be reported in km.

We used this procedure for each investigated HNL PCF and the results can be seen in Figure 3.8 and Figure 3.9.

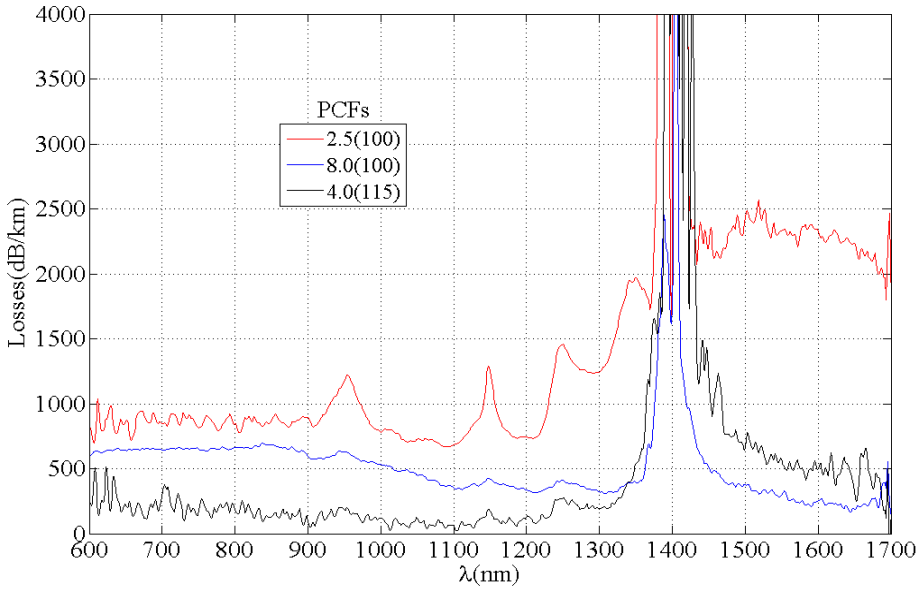

Figure 3.8 Attenuation for 2.5(100), 8.0(100) and 4.0(115) PCFs.

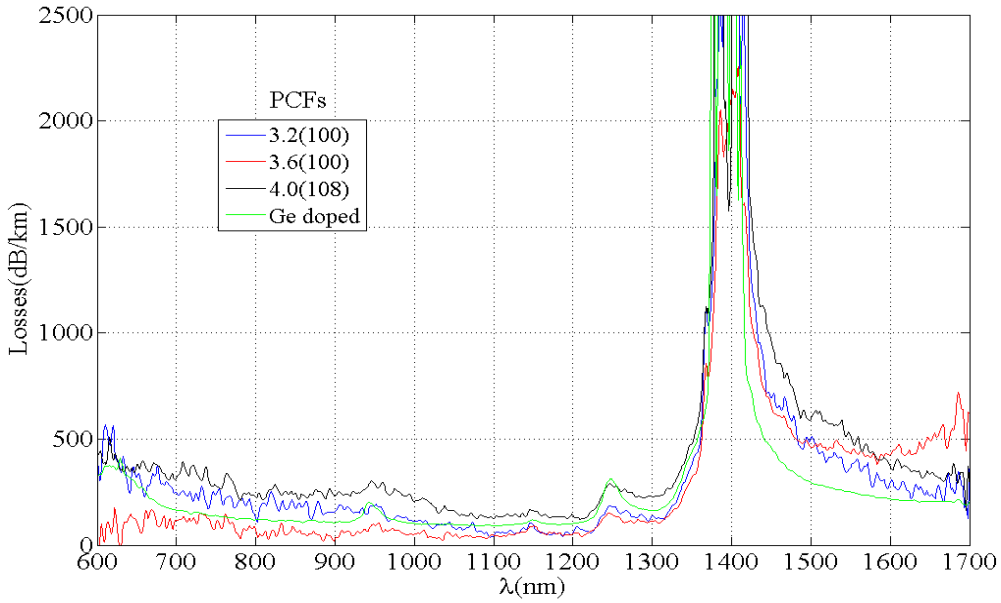

Figure 3.9 Attenuation for 3.2(100), 3.6(100), 4.0(108) and Ge doped PCFs.

The fiber with higher losses was the 2.5(100) and the one with less losses was 3.6(100).

We can notice that all the reported PCF have a strong attenuation peak around 1.38 µm, this is due hydroxyl OH contamination. The OH group is formed by H_20, SiO_2 and SiOH, and they absorb light in specific wavelengths, the most relevant points are 1383, 1246 and 943 nm [62].

3.2.2Numerical aperture

We assumed fundamental mode propagation for measuring the numerical aperture (NA) of each HNL PCF. To do this, we considered light exiting a fiber will have a Gaussian shape, like in Figure 3.10. Ideally, if a screen is placed in a distance D from a fiber-end, a spot will be seen. Then, it is possible to measure the radius d of that light spot.

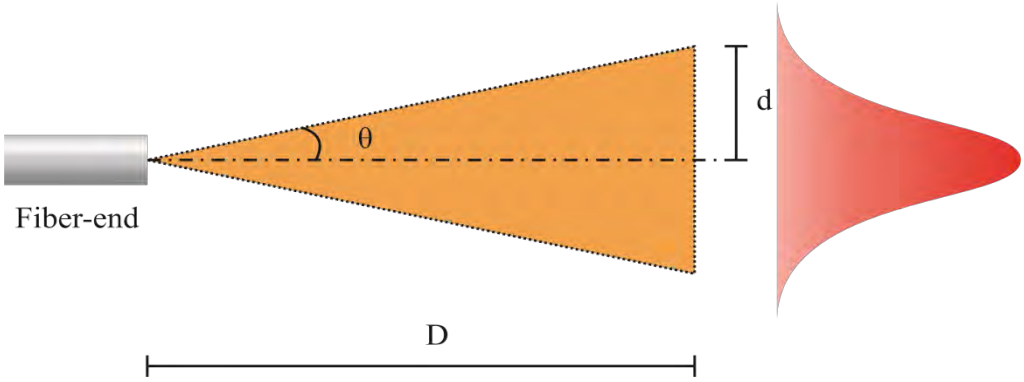

Figure 3.10 Measurement parameters to obtain NA, considering fundamental mode propagating.

Now, using simple trigonometry, the beam divergence angle θ can be found using the next equation:

$$\theta = \arctan\left(\frac{d}{D}\right) \tag{3.2}$$

The acquired results should be similar to the ones from Equation (2.13). Once θ has been computed, the value of its sine is the NA, as explained in Chapter 1.

The experimental setup shown in Figure 3.11 was used to measure NA. Light from an IR ns pulsed laser with a power of about 100 mW at 1064 nm with a repetition rate of 19 kHz was coupled into the different PCFs. To do this, a fiber port (FP1) was used to collimate the laser light, and a set of two mirrors (M1 and M2) were used to modify its optical path until a straight beam was obtained. Then, a second fiber port (FP2) was placed in the center of the path to couple light into the PCF.

The free-end of the PCF was fixed in a displacement base (DB), where the x and y axial positions could be modified. The light was then directed to a small

diaphragm (DP) attached to a photodiode (PH). The DP was made in a piece of dark card with a needle. Finally the PH was connected to a voltmeter.

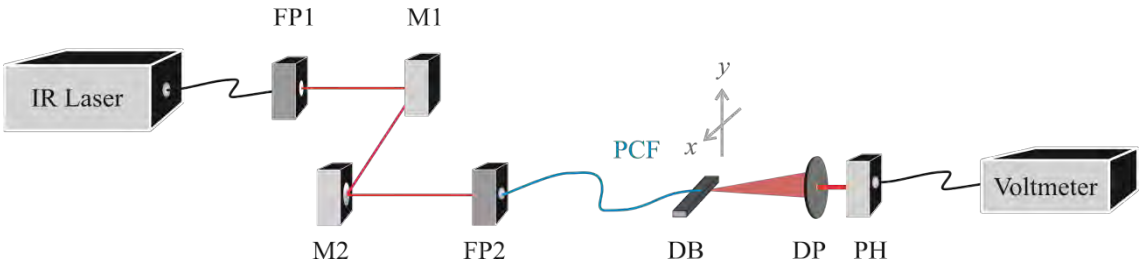

Figure 3.11 Experimental setup for measuring NA of PCFs.

We obtained the output shape for x and y axes using the DB. First, we found the maximum intensity of the light detected by the PH, and we moved it carefully from one side to another. We noticed that there was only one point where the intensity was maximum, and it decreased symmetrically from both sides. For this reason, we decided to measure half of the output beam, starting from the maximum intensity and ending in the last displacement step of the DB. The acquired data was fitted to a Gaussian shape for a posterior processing (for both axes).

To compute the NA, was necessary to find the distances D and d showed in Figure 3.10. In our experimental set up, the distance D is the one between the end of the PCF and the PH; we measured it directly with a vernier caliper for each PCF.

In the case of d, we used the Gaussian fitted curves to compute its diameter. The considered diameter was the one with a relative intensity of 5 %, as shown in Figure 3.12.

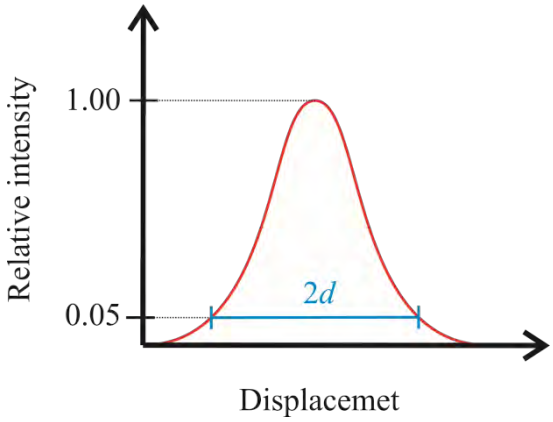

Figure 3.12 Parameter d computed from Gaussian fitted curves.

We placed an attenuator before the FP2 to reduce the coupled power to less than 1 mW, because if high power was coupled, non-linear effects took place and other modes were propagating. We used this procedure to each PCF.

Figures (3.13) to (3.19) show the Gaussian fitting shape for each PCF. Notice that in some cases the difference in x and y axes is considerable, this is due the asymmetry of the fiber core.

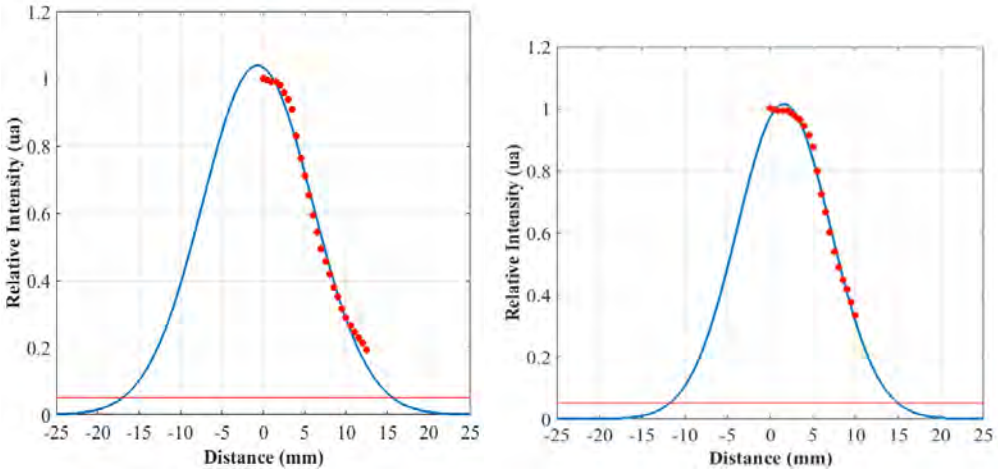

Figure 3.13 Gaussian fitting shape for 2.5(100) PCF output beam. Left for x axis and right to y axis.

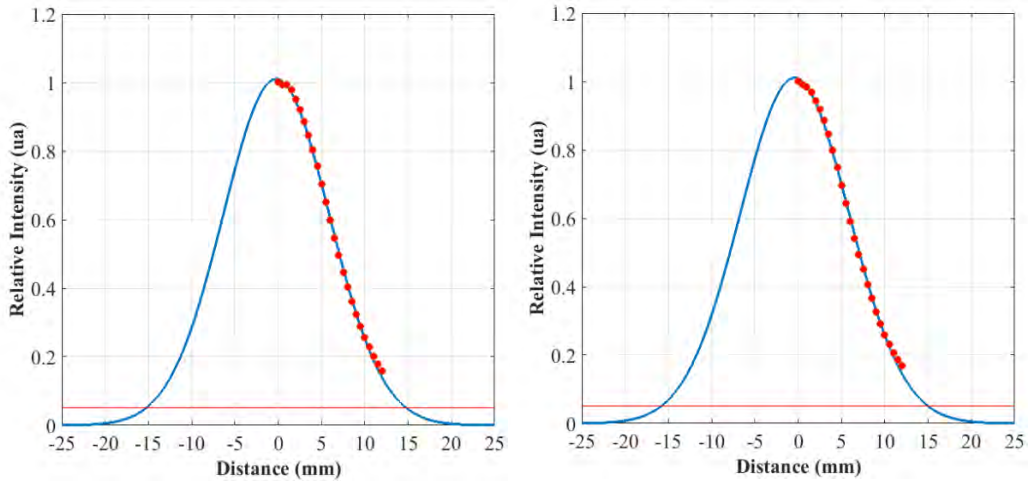

Figure 3.14 Gaussian fitting shape for 3.6(100) PCF output beam. Left for x axis and right to y axis.

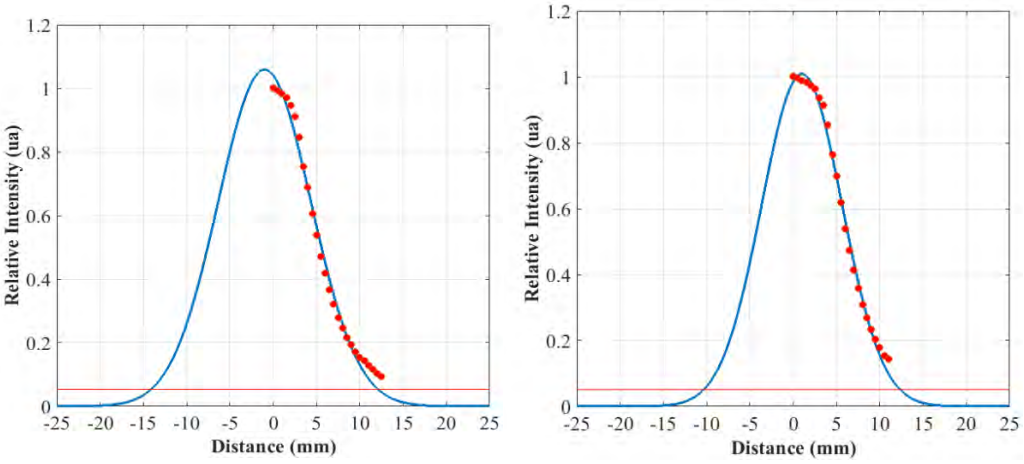

Figure 3.15 Gaussian fitting shape for 4.0(108) PCF output beam. Left for x axis and right to y axis.

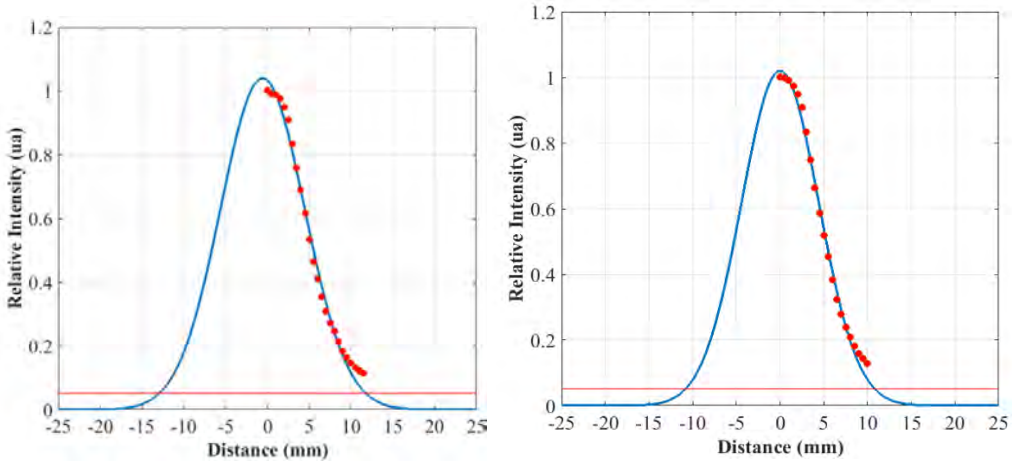

Figure 3.16 Gaussian fitting shape for 3.2(100) PCF output beam. Left for x axis and right to y axis.

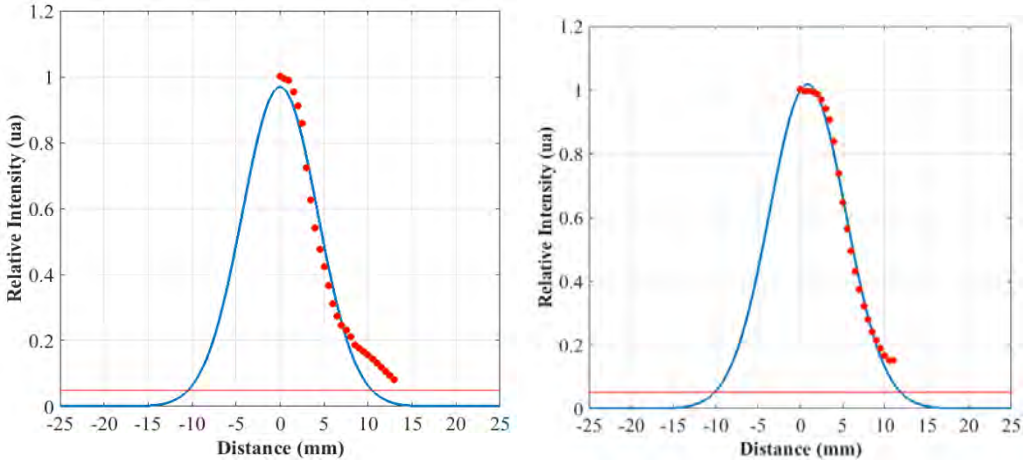

Figure 3.17 Gaussian fitting shape for 4.0(115) PCF output beam. Left for x axis and right to y axis.

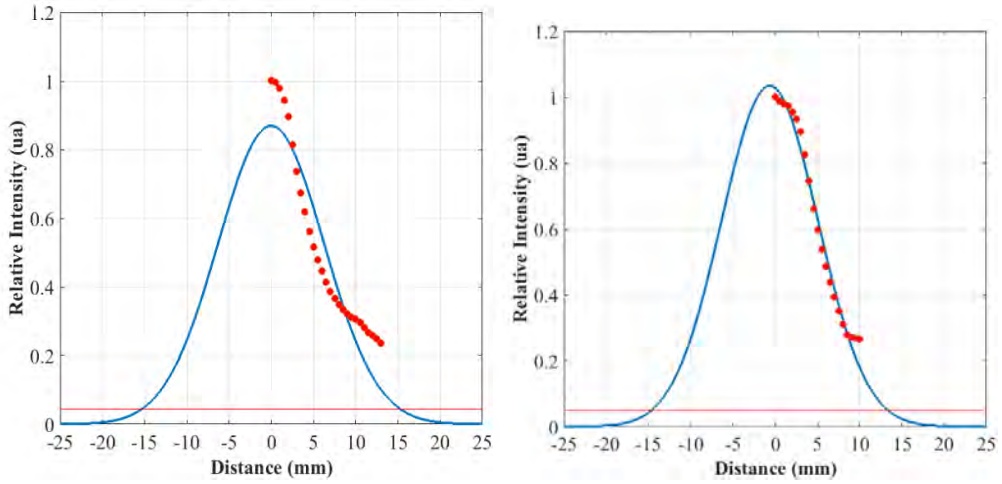

Figure 3.18 Gaussian fitting shape for 8.0(1900) PCF output beam. Left for x axis and right to y axis.

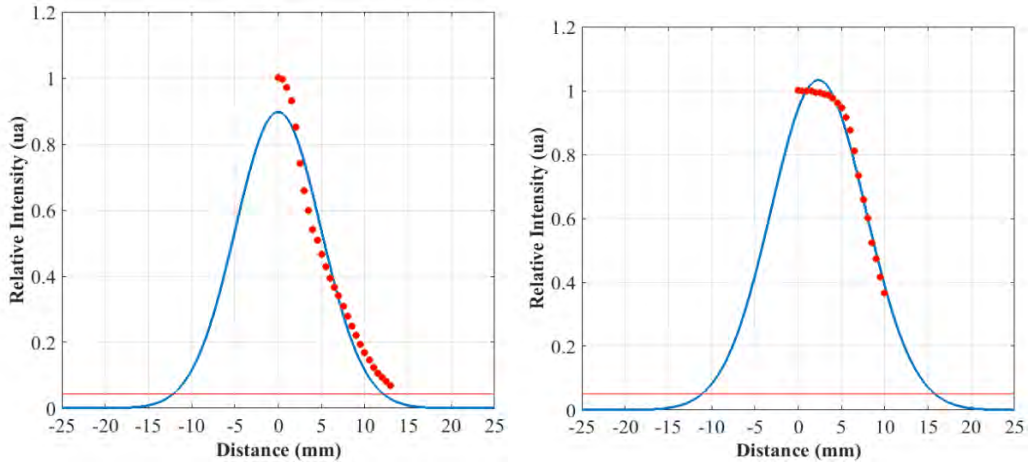

Figure 3.19 Gaussian fitting shape for Ge doped PCF output beam. Left for x axis and right to y axis.

It is possible to see in figures 3.13-3.19 that only 3.6(100) PCF is a single-mode fiber for a wavelength of 1060 nm. All the rest investigated fibers are multimode fibers.

Table 3.3 shows the computed NA using Equation (3.2). To determine the parameter d, we averaged its value in both axes, x and y.

Fiber	Fiber length (m)	Parameter d (mm) (x axis)	Parameter d (mm) (y axis)	Parameter D (mm)	Angle θ (º)	NA
2.5(100)	4.9	16.58	13.40	16.51	42.23	0.6722
3.6(100)	7.3	15.03	15.42	21.80	34.93	0.5726
4.0(108)	10.0	13.14	11.37	18.50	33.52	0.5523
3.2(100)	5.8	12.33	10.83	17.08	34.13	0.5612
4.0(115)	7.5	10.48	11.04	15.75	34.34	0.5641
8.0(1900)	7.3	15.34	13.94	15.75	42.91	0.6808
Ge doped	10.0	12.09	14.72	15.90	40.13	0.6446

Table 3.3 Experimental results to obtain NA for all the PCFs

3.3 Commercial HNL PCFs

So far, we have presented the main properties of HNL PCFs based in theoretical analysis and experimental characterization. Almost all of them were fabricated at CIO, with the stack and draw technique, and their properties are unique. Nowadays, it is possible to find commercial HNL PCFs with fixed geometrical designs; but their prices are high and the variety is limited.

For instance, THORLABS® offers five different types of HNL PCFs, with prices from $657.00 to $1,590.00 USD per meter. Newport® also sells this type of fiber, but only two models with prices of $1,207.50 and $2,875.00 USD per meter. In their datasheets, they report better attenuation than the ones studied in this work. In Figure 3.20, the transmission losses for a Newport NL-PM-750 PCF is shown.

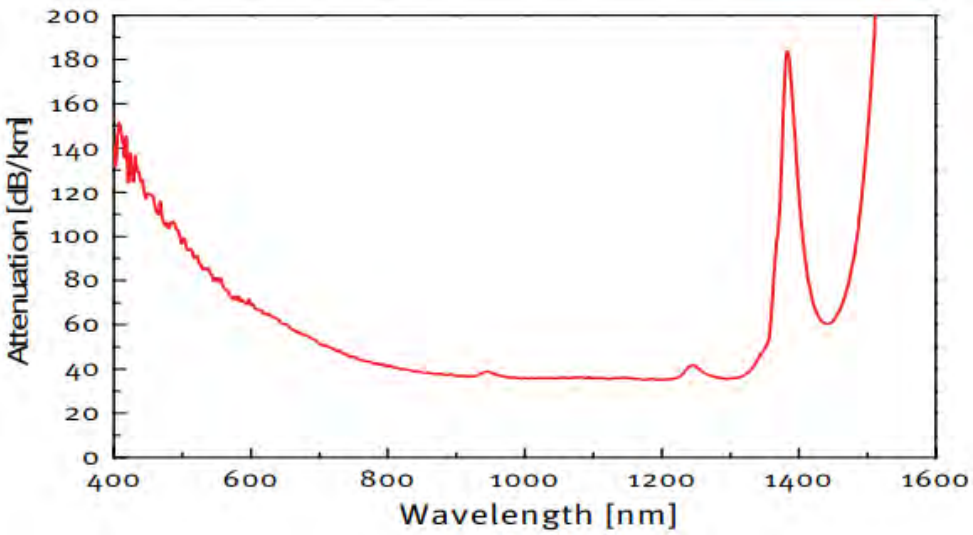

Figure 3.20 Attenuation curve for the commercial PCF: NL-PM-750. Courtesy of Newport.

Compared with our PCF with low losses, the 3.6(100) in Figure 3.9, the smallest attenuation difference takes place in the 0.8 to 1.2 µm wavelength range, with a value of about 10 dB/km. Whereas after 1.3 µm wavelength, the difference is greater. This occurs because the fabrication of commercial fibers takes place possible in a cleaner environment, with less contaminants. The manufacturers usually deliver the HNL PCFs with the face-end sealed, to avoid particles entering in the air holes.

However, the HNL PCFs fabricated in CIO, despite the high enough losses, are suitable for different research purposes. Besides, it is also possible to design them for specific applications, what is impossible with using commercial ones.

Chapter 4
Conclusion

HNL IG PCFs are difficult to fabricate, due to their complicated preform fabrication and also for their two steps of drawing to obtain a small core and very small air hole diameters. For this reason, the prices of commercial HNL PCFs are very expensive (up to 3,000.00 USD per meter). Several PCF fabrication methods are known, each one is more convenient for a specific type of fiber, but the most used one is the stack and draw technique. During the work a strong theoretical background was acquired in the methods of HNL PCF fabrication. We also used the stack and draw technique. It was developed an improved fabrication of composite silica preforms and found an improved regimes for drawing of special (with limited number of air hole rings in the cladding) HNL IG PCFs.

The most attractive characteristic of HNL IG PCFs is the possibility to modify their dispersion properties by only modifying their geometrical parameters: the distance between air holes or pitch Λ and the diameter of these holes d. Several mathematical models were investigated to simulate PCF dispersion properties and we chose one, based on V and W parameters. It is a simple enough and provides good approaches compared with other methods. Using this method, a

MATLAB program was developed to compute the most representative parameters for fabricated PCFs. They are: n_{eff}, n_{FSM}, dispersion properties, mode field diameter and beam divergence. However, this method has a weak point: it assumes that the cladding in the fiber propagates till infinity. In conventional fibers this assumption is not important. But for HNL IG PCFs this method produces some errors at calculation of HNL IG PCFs properties.

A critical point in the theoretic characterization is to measure the HNL IG PCFs geometrical parameters because the used theoretic model is based on their precise dimensions. The most efficient tool to measure them is an atomic force microscope. For this work, all the geometric parameters of our HNL IG PCFs were measured by Dr. Sergio Calixto with a commercial scanning atomic force microscope (Digital Instruments) with a resolution of 50 nm for 30 µm X 30 µm images. Unfortunately, dispersion measurements were not performed because the equipment available for such measurements is absent in CIO. Then, it is logic to consider the theoretical dispersion curves computed in this work; where it is possible to find one of the most important parameter of HNL PCFs: zero wavelength dispersion.

Besides the intrinsic material absorption, OH contamination and impurities absorptions; the attenuation in the fabricated HNL PCFs is high enough due to their small core and hole sizes and also due to not clean enough atmosphere in the CIO fabrication laboratory. The measured attenuation varied from 40 to 1000 dB/km in the 0.6 to 1.2 µm wavelength range, depending from the analyzed HNL PCF. For larger wavelengths, the losses were much higher, reaching attenuations peaks superior to 2500 dB/km.

Due to their high losses, HNL PCFs are not suitable for long power transmissions, but as it will be shown later, they are useful for application where high non-linearity is required. One of the most exploited property of fabricated HNL PCFs is the supercontinuum (SC) generation. The HNL PCFs fabricated and characterized in this work are expected to produce a good SC using a pump source near their zero wavelength dispersion; for instance, at using an IR ns laser at 1064 nm wavelength.

Finally, during numerical aperture measurements with an IR ns laser at 1064 nm wavelength, the main issue was to couple the light into the core of the HNL PCFs. Once it was coupled, the high power within the core induced non-linear effects, leading to beam broadening. For this reason, it was necessary to use an attenuator to reduce the power, otherwise the Gaussian beam would be modified.

Finally, it is important to point out that only in a few locations around the world the design and fabrication of PCFs is carried out. The relevance of this work lies in the acquirement of knowledge and skills in these topics, more specifically in HNL IG PCFs.

As a future work, it is necessary to propose a new geometry of HNL IG PCFs in order to have a ZVD of fibers near to the pump source. Another proposal is to fabricate HNL IG PCFs with a doped core to increase the nonlinear properties of these fibers and to generate a broader supercontinuum with high supercontinuum generation efficiency.

Now fabrication of HNL IG PCFs is very complicated process. It is very important to simplify this process.

References

[1] M.J. Gander, R. McBride, J.D.C. Jones, D. Mogilevtsev, T.A. Birks, J.C. Knight, and P.S.J. Russell, "Experimental measurement of group velocity dispersion in photonic crystal fibre," Electron. Lett., vol. 35, no. 1, p. 63-64, 1999.

[2] J.K. Ranka, R.S. Windeler, and A.J. Stentz, "Visible continuum generation in air-silica microstructure optical fibers with anomalous dispersion at 800 nm," Opt. Lett., vol. 25, no. 1, p. 25-27, 2000.

[3] J.C. Knight, J. Arriaga, T.A. Birks, A. Ortigosa-Blanch, W.J. Wadsworth, and P.S.J. Russell, "Anomalous dispersion in photonic crystal fiber," IEEE Photon. Technol. Lett. , vol. 12, no. 7, p. 807-809, 2000.

[4] Z. Holdynski, M. Napierala, P. Mergo, and T. Nasilowski, "Experimental investigation of supercontinuum generation in photonic crystal fibers pumped with sub-ns pulses," J. Lightw. Technol., vol. 33, no. 10, p.2106-2110, 2015.

[5] K.M. Hilligsoe, T.V. Andersen, H.N. Paulsen, C.K. Nielsen, K. Molmer, S. Keiding, et al., "Supercontinuum generation in a photonic crystal fiber with two zero dispersion wavelengths," Opt. Express, vol. 12, no. 6, p. 1045-1060, 2004.

[6] A. Kudlinski, S.F. Wang, A. Mussot, and M. Conforti., "Soliton annihilation into a polychromatic dispersive wave," Opt. Lett., vol. 40, no. 9, p. 2142-2145, 2015.

[7] M.L.V. Tse, P. Norak, J.H.V. Price, F.Poletti, F. He, and D.J. Richardson, "Pulse compression at 1.0 µm in dispersion-decreasing holey fibers," Opt. Lett., vol. 31, no. 23, p. 3504-3506, 2006.

[8] J.C. Travers, J.M. Stone, A.B. Rulkov, B.A. Cumberland, A.K. George, S.V. Popov, et al., "Optical pulse compression in dispersion decreasing photonic crystal fiber," Opt. Express, vol. 15, no. 20, p. 13203-13211, 2007.

[9] K.P. Hansen, "Dispersion flattened hybrid-core nonlinear photonic crystal fiber," Opt. Express, vol. 11, no. 13, p. 1503-1509, 2003.

[10] F. Poli, A. Cucinotta, S. Sellery, and A.H. Bouk, "Tailoring of flattened dispersion in highly nonlinear photonic crystal fibers," IEEE Photon. Technol. Lett. , vol. 16, no. 4, p. 1065-1067, 2004.

[11] M.L.V. Tse, P. Horak, F. Poletti, N.G.R. Broderick, J.H.V. Price, J.R. Hayes, and D.J. Richardson, "Supercontinuum generation at 1.06μm in holey fibers with dispersion flattened profiles," Opt. Express, vol. 14, no. 10, p. 4445-4451, 2006.

[12] Knight J.C. and Wadsworth W.J., "Silica fibres for supercontinuum generation," in [Supercontinuum Generation in Optical Fibers], Dudley J.M. and Taylor J.R., Eds, Cambridge Univ. Press, 62-81 (2010).

[13] A. Kudlinski, A.K. George, J.C. Knight, J.C. Travers, A.B. Rulkov, S.V. Popov, and J.R. Taylor, "Zero dispersion wavelength decreasing photonic crystal fibers for ultraviolet-extended supercontinuum generation," Opt. Express, vol. 14, p. 5715-5722, 2006.

[14] B.A. Cumberland, J.C. Travers, S.V. Popov, and J.R. Taylor, "29W High power CW supercontinuum source,"Opt. Express, vol. 16, p. 5954-5962, 2008.

[15] F. Poli, A. Cucinotta and S. Selleri, Photonic Crystal Fibers, Properties and Applications, Springer Series in Materials Science 102, p. 1. (2007).

[16] A. Ghatak, K. Thyagarajan, Introduction to Fiber Optics, Cambridge University Press, p. 29. (1998).

[17] J. Downing, Fiber optic communications, Cengage Learning, p. 67, (2004).

[18] F. Zolla, G. Renversez, A. Nicolet, B. Kuhlmey, S. Guenneau, D. Felbacq and S. Leon-Saval, Foundations of Photonic Crystal Fibres, Imperial College Press, 2nd edition, p. 7, (2012).

[19] T. Okoshi, Optical Fibers, Academic Press, New York, (1982).

[20] R. S. Quimby, Photonics and Lasers: An Introduction, Wiley-Interscience, p. 62-63, (2006)

[21] J. Downing, Fiber optic communications, Cengage Learning, p. 73, (2004).

[22] F. Zolla, G. Renversez, A. Nicolet, B. Kuhlmey, S. Guenneau, D. Felbacq and S. Leon-Saval, Foundations of Photonic Crystal Fibres, Imperial College Press, 2nd edition, p. 8, (2012).

[23] T. Okoshi, Optical Fibers, Academic Press, New York, p. 72 (1982).

[24] J. Downing, Fiber Optic Communications, Cengage Learning, p. 79, (2004).

[25] S. John, Strong localization of photons in certain disordered dielectric superlattices, Physical Review Letters 58, pp. 2486-2489, (1987).

[26] E. Yablonovitch, Inhibited spontaneous emission in solid-state physics and electronics, Physical Review Letters 58, pp. 2059-2062, (1987).

[27] A. Bjarklev, J. Broeng, A. Sanchez, Photonic Crystal Fibres, Springer, p. 2, (2003).

[28] J. C. Knight, T. A. Birks, P. St. J. Russell, and D. M. Atkin, All-silica single-mode optical fiber with photonic crystal cladding, Opt. Lett. 21, 1547-1549 (1996)

[29] C.M. Soukoulis. Photonic band gaps and localization. In NATO Advanced Study Institute series. Series B, Physics. Plenum, (1993).

[30] F. Poli, A. Cucinotta and S. Selleri, Photonic Crystal Fibers, Properties and Applications, Springer Series in Materials Science 102, pp. 1-2. (2007).

[31] A. Bjarklev, J. Broeng, A. Sanchez, Photonic Crystal Fibres, Springer, pp. 9-11, (2003).

[32] J. C. Knight, T. A. Birks, R. F. Cregan, P. S. Russel, J. P. de Sandro, Large mode area photonic crystal fibre, IEE Electronics Letters, Vol. 34, No.13, pp. 1347-1348, (1998).

[33] K. P. Hansen, J. R. Jensen, C. Jacobsen, H. R.Simonsen, J. Broeng, P. M. W. Skovgaard, A. Bjarklev, Hihgly nonlinear photonic crystal fiber with zero dispersion at 1.55 μm, OFC'2002, postdeadline paper, paper FA9, pp. 1-3, (2002).

[34] J. Broeng, S. E. Barkou, T. Sondergaard, A. Bjarklev, Analysis of air-guiding photonic bandgap fibers, Optic Letters, Vol. 25, No. 2, pp. 96-98, (2000).

[35] A.N. Naumov, A. M. Zheltikov, Optical harmonic generation in hollow-core photonic-crystal fibres: analysis of optical losses and phase-matching conditions, Quantum Electronics, Vol. 32, No. 2, pp. 129-134, (2002).

[36] F. Zolla, G. Renversez, A. Nicolet, B. Kuhlmey, S. Guenneau, D. Felbacq and S. Leon-Saval, Foundations of Photonic Crystal Fibres, Imperial College Press, 2nd edition, pp. 20-22, (2012).

[37] A. W. Snyder, J. D. Love, J. D. Optical Waveguide Theory, Chapman and Hall, New York, (1983).

[38] K. Saitoh, M. Koshiba, Empirical relations for simple design of photonic crystal fibers, Opt. Express 13, 267-274 (2005).

[39] C. K. Kao, Optical Fibre, Peter Peregrinus, London, (1988).

[40] F. Zolla, G. Renversez, A. Nicolet, B. Kuhlmey, S. Guenneau, D. Felbacq and S. Leon-Saval, Foundations of Photonic Crystal Fibres, Imperial College Press, 2nd edition, pp. 61-72, (2012).

[41] J. C. Knight, T. A. Birks, P. St. J. Russell, D. M. Atkin, All-silica single-mode optical fiber with photonic crystal cladding, Opt. Lett. 21, 1547-1549 (1996).

[42] G. Barton, M. van Eijkelenborg, G. Henry, M. Large, J. Zagari, Fabrication of microstructured polymer optical fibres, Optical Fibre Technology 10, pp. 325-335, (2004).

[43] V. Kumar, A. George, W. Reeves, J. Knight, P. St. J. Russell, F. Omenetto, and A. Taylor, Extruded soft glass photonic crystal fiber for ultrabroad supercontinuum generation, Opt. Express 10, 1520-1525 (2002).

[44] R. T. Bise, D. Trevor, Solgel-Derived Microstructured Fibers: Fabrication and Characterization, in Optical Fiber Communication Conference and Exposition and The National Fiber Optic Engineers Conference, Technical Digest (CD) (Optical Society of America, 2005), paper OWL6.

[45] A. Bétourné, V. Pureur, G. Bouwmans, Y. Quiquempois, L. Bigot, M. Perrin, M. Douay, Solid photonic bandgap fiber assisted by an extra air-clad structure for low-loss operation around 1.5 μm, Opt. Express 15, 316-324 (2007)

[46] M. V. Pereira, Fabricación e Investigación de Fibras de Cristal Fotónico (Microestructuradas) con Núcleo de Gran Área, Centro de Investigaciones en Óptica, (2012).

[47] S. Coen, A. H. Lun Chau, R. Leonhardt, J. D. Harvey, J. C. Knight, W. J. Wadsworth, P. St. J. Russell, Supercontinuum generation by stimulated Raman scattering and parametric four-wave mixing in photonic crystal fibers, J. Opt. Soc. Am. B 19, 753-764 (2002).

[48] J. K. Ranka, R. S. Windeler, A. J. Stentz, Visible continuum generation in air–silica microstructure optical fibers with anomalous dispersion at 800 nm, Opt. Lett. 25, 25-27 (2000).

[49] I. Hartl, X. D. Li, C. Chudoba, R. K. Ghanta, T. H. Ko, J. G. Fujimoto, J. K. Ranka, R. S. Windeler, Ultrahigh-resolution optical coherence tomography using continuum generation in an air–silica microstructure optical fiber, Opt. Lett. 26, 608-610 (2001).

[50] G. P. Agrawal, Nonlinear Fiber Optics, Academic, New York, (1989).

[51] A. Bjarklev, J. Broeng, A. Sanchez, Photonic Crystal Fibres, Springer, p. 234, (2003).

[52] V. Finazzi, T. M. Monro, D. J. Richardson, The role of confinement loss in highly nonlinear silica holey fibers, IEEE Photonics Technology Lett. 15 No. 9, (2003).

[53] S.G. Johnson, J.D. Joannopoulos, Block-iterative frequency-domain methods for Maxwell's equations in a planewave basis, Opt. Express 8, 173-190 (2001).

[54] T.P. White, B.T. Kuhlmey, R.C. McPhedran, D. Maystre, G. Renversez, C.M. de Sterke, L.C. Botten, Multipole method for microstructured optical fibers. I. Formulation, J. Opt. Soc. Am. B 19, 2322-2330, (2002).

[55] M. Koshiba, Full-vector analysis of photonic crystal fibers using the finite element method, IEICE Trans. Electron. E85-C, 881-888 (2002).

[56] K. Saitoh and M. Koshiba, Full-vectorial imaginary-distance beam propagation method based on finite element scheme: Application to photonic crystal fibers, IEEE J. Quantum Electron. 38, 927-933 (2002).

[57] K. Saitoh and M. Koshiba, Empirical relations for simple design of photonic crystal fibers, Opt. Express 13, 267-274 (2005).

[58] N. A. Mortensen, J. R. Folkenberg, M. D. Nielsen, K. P. Hansen, Modal cutoff and the V parameter in photonic crystal fibers, Opt. Lett. 28, 1879 (2003).

[59] D. Marcuse, Loss Analysis of Single-Mode Fiber Splices, Bell Syst. Tech. J. 56, 703 (1977).

[60] M. Koshiba and K. Saitoh, Applicability of classical optical fiber theories to holey fibers, Opt. Lett. 29, 1739-1741 (2004).

[61] G. Ghosh, Sellmeier coefficients and dispersion of thermo-optic coefficients for some optical glasses, Appl. Opt. 36, 1540-1546 (1997).

[62] O. Humbach, H. Fabian, U. Grzesik, U. Haken, W. Heitmann. Analysis of OH absorption bands in synthetic silica. Journal of Noncrystalline Solids, 203:19–26, (1996).

[63] V.P. Minkovich, A.V. Kir'yanov, A.B. Sotsky, and L.I. Sotskaya, "Large-mode-area holey fibers with a few air channels in cladding: modeling and experimental investigation of modal properties," J. Opt. Soc. Am. B, vol. 21, no. 6, pp.1161-1169 (2004).